Universidade de Aveiro Departamento de Engenharia Cerâmica e do Vidro
2011

Alena Kuznetsova

SÍNTESE E CARATERIZAÇÃO DE NANORESERVATÓRIOS INORGÂNICOS

Universidade de Aveiro Departamento de Engenharia Cerâmica e do Vidro
2011

Alena Kuznetsova

SÍNTESE E CARATERIZAÇÃO DE NANORESERVATÓRIOS INORGÂNICOS

Dissertação apresentada à Universidade de Aveiro para cumprimento dos requisitos necessários à obtenção do grau de Mestre em Engenharia de Materias, realizada sob a orientação científica do Doutor Mikhail Zheludkevich, Investigador Auxiliar do Departamento de Engenharia Cerâmica e do Vidro da Universidade de Aveiro e do Doutor João André da Costa Tedim, Bolseiro de Pós-Doutoramento do Departamento de Engenharia Cerâmica e do Vidro-CICECO da Universidade de Aveiro

o júri

presidente

Prof. Doutor Mário Guerreiro Silva Ferreira
Professor Catedrático do Departamento de Engenharia Cerâmica e do Vidro da Universidade de Aveiro

Prof. Doutor Pedro Manuel Lima de Quintanilha Mantas
Professor Auxiliar do Departamento de Engenharia Cerâmica e do Vidro da Universidade de Aveiro

Doutora Maria de Fátima Grilo da Costa Montemor
Investigadora Auxiliar do Departamento de Engenharia Química e Biológica do Instituto Superior Técnico

Doutor Mikhail Larionovich Zheludkevich
Investigador Auxiliar do Departamento de Engenharia Cerâmica e do Vidro da Universidade de Aveiro

Doutor João André da Costa Tedim
Bolseiro de Pós-Doutoramento do CICECO da Universidade de Aveiro

agradecimentos

Os meus agradecimentos vão para os meus orientadores Dr. Mikhail Zheludkevich e Dr. João Tedim, pela orientação e o apoio incondicional, em todos os momentos.
Ao Dr. Andrei Salak, Aleksey Lisenkov, Eng.ª Célia Cristina Moreira Pereira Miranda, Eng.ª Ana Sofia Marques Ribeiro, Eng.ª Dulce Helena Ferreira Martins Gomes Teixeira e a todos os meus colegas de grupo de SECOP, trabalhadoras da Secretaria do Departamento de Engenharia Cerâmica e do Vidro da Universidade de Aveiro: Dra. Alexandra Sílvia Vieira Do Vale Romana Martins, Maria Luísa Pinto Oliveira Costa, Tatsiana Zhaludkevich pela ajuda e a colaboração.
Por último agradeço à minha família, ao meu marido e a todos os meus amigos pelo apoio e a inspiração.

palavras-chave

Hidróxido duplo lamelares, síntese, coprecipitação, inibidor de corrosão, dispersão dinâmica de luz, difração de raio X.

resumo

O principal objectivo do presente trabalho consiste na preparação de nanoreservatórios inorgânicos baseado em hidróxidos duplos lamelares (LDHs) para intercalação de espécies activas, nomeadamente inibidores de corrosão. LDHs são conhecidos como estruturas inorgânicas constituídas por camadas de hidróxidos de catiões metálicos com carga positiva compensada pela presença de aniões e moléculas de água no espaço entre as referidas camadas. A característica mais importante deste material é a sua capacidade de permuta aniónica. Neste trabalho os LDHs foram preparados de acordo com duas metodologias: coprecipitação, e calcinação-rehidratação de LDHs comerciais. No caso dos LDHs obtidos por coprecipitação a intercalação de inibidores efectuou-se por reacção de permuta aniónica, enquanto que no caso de LDHs obtidos por calcinação-rehidratação, a intercalação do inibidor é intrínsica ao passo de rehidratação/reconstrução. Estrutura, morfologia e propriedades coloidais dos LDHs obtidos foram caracterizadas por difracção de raios-X (DRX), espectroscopia de infravermelho por transformada de Fourier (FTIR), microscopias eletrónicas (SEM), dispersão dinâmica de luz (DLS), análise química (ICP-OES) e térmica (termogravimetria, TG). No caso de LDHs sintetizados por coprecipitação as condições de síntese, nomeadamente tratamento hidrotérmico, temperatura, pH e presença de surfactantes, foram optimizadas para obter LDHs com as características adequadas para incorporação em revestimentos anticorrosão (cristalinidade, tamanho das partículas).

keywords

Layered double hydroxide, synthesis, coprecipitation, corrosion inhibitor, dinamic light scattering, X-ray diffraction.

abstract

The main objective of the present work is the preparation of inorganic nanoreservoirs based on layered double hydroxides (LDHs) for intercalation of active species, namely corrosion inhibitors.

Layered double hydroxides are known as structures consisting of positively-charged, mixed-metal hydroxide layers, between which balancing anions and water molecules are found. The most important feature of this material is its anion exchange ability. LDHs have been prepared by two methodologies: coprecipitation and calcination-rehydration of commercial LDHs. In the case of LDHs prepared by coprecipitation, the subsequent intercalation of corrosion inhibitors was performed by anion-exchange reaction, while in the case of calcination-rehydration the intercalation of inhibitor is intrinsic to rehydration/reconstruction step. Structure, morphology and colloidal properties of the resulting nanocontainers have been characterized using X-ray diffraction (XRD), Fourier transform infrared specroscopy FTIR, electron microscopies (SEM), dynamic light scattering (DLS), chemical (inductively coupled plasma optical emission spectrometry, ICP-OES) and thermal analysis (thermogravimetry, TG). In the case of LDHs synthesized by coprecipitation, the synthesis conditions, namely hydrothermal treatment, temperature, pH and presence of surfactant were optimized with the aim to obtain LDHs suitable for incorporation in anticorrosion coatings (crystallinity, particle size).

Contents

Introduction

In everyday life people are surrounded by metallic structures. Buildings, bridges, automobiles, passenger trains, ships, docks, storage tanks are made from different types of steel. Aluminum alloys are also applied in various fields, from aircraft industries and finishing to food containers and electronic equipment. Copper is used for the construction of water pipes and electrical connectors. Metals can also be associated with biomedical applications, namely for hip or kneel replacements, for construction of arterial stents, surgical plates, screws, and wires [1]. However, all common metals have a tendency to react with the environment in different extents and rates. In general, the process of degradation of materials (in particular, metals) by interaction with the environment is called corrosion [2]. In addition, the costs connected with repairing and maintenance of damaged structures caused by corrosion is large (3-4% of GNP in industrialised countries) [1, 2]. Hence, corrosion protection is a very important and actual aspect.

There are many corrosion control methods, among them are the following: the use of inorganic, organic or metallic coatings; cathodic and anodic protection; the use of corrosion inhibitors and removal of aggressive components. The choice of the most appropriate method depends on the type of metals or alloys and the features of the surrounding environment. Often, an effective protection is achieved when different methods are combined (e.g. cathodic protection together with corrosion inhibitors and coatings [3]).

The utilisation of chromates as corrosion inhibitors has been considered among the most effective species for corrosion protection. Chromate anions can act simultaneously as anodic and cathodic inhibitor and reduce the overall electrochemical activity on the surface. Even a low concentration of chromates is enough to obtain anticorrosion activity. These anions can passivate metals after being released from chromate-based coatings (conversion coatings prepared via anodization), because of the reaction with the actively corroding sites. Some chromate-based pigments (as $BaCrO_4$ and $SrCrO_4$) can also be introduced into polymer matrices, revealing an effective corrosion inhibition for a wide range of metals [4]. All these characteristics made chromates very attractive for active corrosion protection. However, since 2007 strict law regulations have forbidden the

application of Cr^{6+}-containing species in corrosion protection systems, activating intense research for finding "greener" approaches for an effective replacement of chromates. The list of currently available inhibitors for different applications is wide. Among them one may find silicates, polyphosphates, benzotriazole, sodium mercaptobenzothiazole, different amines, amides etc. [1]. One strategy to obtain proper corrosion protection has been accomplished by combination of different corrosion inhibitors in the same system. There are patents for corrosion protection in cooling water systems containing mixtures of inhibitors (so-called inhibitors packages). For example, Li et al. have patented an inhibitor package of sodium silicate, sodium tungstate, sodium phosphate/hexametaphosphate and benzotriazole/mercaptobenzothiazole along with an acrylic co-polymer for desalted circulating cooling water system [6]. Cao has patented another combination of inhibitors: sodium gluconate, benzotriazole, tolyltriazole, molybdate, tungstate and $ZnSO_4$ [7]. Tayler et al. have studied the synergetic inhibition of anodic (vanadates, molybdates, tungstates, phosphates, borates) and cathodic inhibitors (cerium, yttrium, lanthanum, europium, gadolinium, neodymium) as possible substitutes for chromates [8]. Aballe and collegues have also studied corrosion inhibition of Al-Mg alloy (AA5083) by binary solution of cerium and lanthanum chlorides [9].

One of the most common approaches for protection of metals and corresponding alloys is based on application of organic coatings with corrosion inhibitors. The coating acts as a barrier against aggressive species (passive protection) while the inhibitors act actively in the corrosion processes at the metal surface (active protection). Nevertheless, the direct dispersion of corrosion inhibitor in organic coating matrices can lead to the detrimental interaction between them, osmotic blistering due to the solubility of inhibitors, and spontaneous leaching of inhibitors that may exhaust the active protection functionality and thus reduce the service life of metallic substrates. These negative results can be suppressed, or at least minimised, if the active species are loaded in inert hosting nanostructures, capable of entrapping the corrosion inhibitors and releasing them only when specific conditions in the surrounding media coinciding with corrosion initiation are verified, namely pH changes and presence of aggressive species (e.g. Cl^-, SO_4^{2-}) [5]. These are commonly designated as micro and nanocontainers. Among them one may find mixed-oxide nanoparticles, β-cyclodextrin-inhibitor complexes or hollow propylene fibers [10]. Additionally, the layer-by-layer (LbL) technique which allows the deposition of oppositely

charged species on substrates has been suggested as an interesting way of synthesising nanocontainers with controlled storage-release properties. For example, corrosion inhibitors can be entrapped between polyelectrolyte multilayers and consequently these nanoreservoirs can be incorporated in anticorrosion protective films [10, 11]. Application of polyelectrolyte self-assembly method with different template cores [12, 13] allows the preparation of a variety of nanocontainers that can be potentially interesting for exploration in corrosion science since the permeability of the polyelectrolytes is dependent on pH, an important parameter for the occurrence of corrosion processes.

Ion exchangers are another example of 'smart' reservoirs for the release of species. In this case the release is triggered by the presence of ions in the neighbouring environment. These include cation-exchangers such as bentonite and anion-exchangers like layered double hydroxides (LDHs). LDHs are particularly attractive systems because of their environmental friendly properties, possibility of intercalation of different types of organic or inorganic anions into their structure, simplicity and low-cost of preparation.

Objectives

The main goal of the present work is to prepare of inorganic nanoreservoirs based on layered double hydroxides with active species - corrosion inhibitors. This is accomplished by completion of the following objectives:

-To synthesize different inorganic, nanostructured materials to be used as reservoirs for corrosion inhibitors;

-To intercalate/load active species (corrosion inhibitors) in the inorganic hosting structures;

-To perform structural, morphological and compositional characterization of the obtained reservoir/inhibitor systems.

Chapter 1. State of the art

1.1. Structure of LDHs

Layered materials like clay minerals, metal phosphates and phosphonates, graphite among others are attractive materials as host structures for intercalation of guest molecules, together with the possibility of exchanging ions [14, 15]. Another example of layered structures is the layered double hydroxides (LDHs). They exist as occurring materials in nature, like hydrotalcite ($[Mg_6Al_2(OH)_{16}CO_3 \cdot 4H_2O]$) and pyroaurite ($[Mg_6Fe_2CO_3(OH)_{16} \cdot 4H_2O]$), but can also be obtained synthetically [16]. In the laboratory they were prepared in 1942 by Feitknecht through a reaction between diluted aqueous metal salt solutions and base. However, their structural characterization has only started on the 1960-s [14, 16].

LDHs are crystalline inorganic structures that consist of stacks of positively-charged, mixed-metal hydroxides separated by galleries where anionic species and solvent molecules can be intercalated [14, 18]. The LDH structure is based on the brucite [$Mg(OH)_2$] structure, where divalent cations are substituted by trivalent ones, with the layers of hydroxide, becoming positively charged, which is balanced by presence of anions and water molecules within the interlayer space. The general formula of LDH is the following [14]:

$$[M^{2+}_{1-x} M^{3+}_{x}(OH)_2]A^{n-}_{x/n} \cdot mH_2O \qquad (1)$$

where,

M^{2+}, M^{3+} - divalent and trivalent cations; x is the ratio between di-and trivalent metals $M^{3+}/(M^{2+} + M^{3+})$;

A^{n-} anion with the valence n.

Schematically, the LDH structure is presented in Figure 1.1.1.:

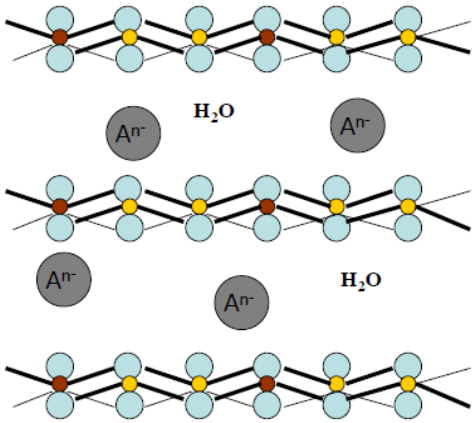

Figure 1.1.1. Scheme of the LDH structure

Different ions can be used as M^{2+} and M^{3+}, as long as their ionic radii do not differ in a large extent from the radius of Mg^{2+} (0.65 Å), to facilitate their accommodation in the holes of close-packed OH groups in the hydroxide layers for the LDH formation. These include Mg^{2+}, Zn^{2+}, Fe^{2+}, Co^{2+}, Cu^{2+}, Ni^{2+}, Cd^{2+}; Al^{3+}, Cr^{3+}, Ga^{3+}, Fe^{3+} [14, 16]. In addition to M^{2+}/M^{3+}-LDHs types, other compositions of LDHs have also been prepared. Porta [19] has successfully synthesized hydrotalcite like materials composed of mixtures of divalent and trivalent ions (Cu/Zn/Co/Al/Cr). Another interesting type of LDHs contains monovalent and trivalent matrix cations, ($[LiAl_2(OH)_6]^+A^-\cdot mH_2O$), where sheets of aluminium octahedra with vacancies are filled by lithium atoms [14, 16]. Besides, trials of preparation of LDHs containing rare-earth metals, including Ce^{3+}, Zr^{4+} have been published as well [20, 21, 22].

In the LDHs structure hydroxide layers are close packed. In the (110) plane all sites can be represented as A, B, C (depending on the lattice translations-1/3, 2/3, 0, 2/3,1/3,0). Analogously, a, b, c can describe the position of octahedral holes which are occupied by metal cations. Hence, a structure of a single brucite layer can be represented as, for example, AbC, (if close packed hydroxyls are situated in A and C sites, therefore, the cations occupy the b sites). Moreover, AbC sheets can be stacked in various ways, resulting in polytypism [16]. *Polytypism phenomenon* consists of the existence of an

element or compound in several structural modifications with difference in the stacking sequence, but with the identical (or near identical) structure and composition [14].

All polytypes can be classified in the frame of the number of stacked sheets along the c axis in the unit cell. For instance, if the opposite hydroxyl groups of adjacent layers lie vertically above one another (all are in C sites), a trygonal prismatic arrangement occurs (denoted as =). On the other hand, if OH groups are offset (one layer is in C sites and others are in A or B sites), six hydroxyls form an octahedral arrangement (denoted as ~). Brucite itself can be described as [16]:

…AbC~AbC… (**1H**)

Where 1H means:

H-stacking sequence with hexagonal structure;

1-one layer polytype;

For LDHs the following types of stacking are usually found: 3R and 2H [26]. There are three possible two-layer polytypes with hexagonal stacking of sheets:

…AbC=CbA=AbC… (**$2H_1$**)

…AbC~AcB~AbC… (**$2H_2$**)

…AbC~BcA=AbC… (**$2H_3$**)

In $2H_1$ polytype all cations occupy b sites, whereas for other polytypes cations alternate between b and c sites. In addition in $2H_1$ and $2H_2$ polytypes interlayers are all prismatic and octahedral respectively, while $2H_3$ contains both of these interlayer arrangement types. The possible three-layer polytypes with rhombohedral symmetry are presented below:

…AbC=CaB=BcA=AbC… (**$3R_1$**)

…AbC~BcA~CaB~AbC… (**$3R_2$**)

The remaining seven possible three-layer stackings have hexagonal symmetry [16]:

…AbC~AcB~AcB~AbC… (**$3H_1$**)

…AbC~AcB~CaB~AbC… (**$3H_2$**)

…AbC~AcB=BcA~AbC… (**$3H_3$**)

…

For $3R_1$, $3R_2$ and $3H_2$ polytypes cations are distributed among all possible sites a, b, c. On the other hand, for different polytypes the interlayers can all be prismatic ($3R_1$) or octahedral ($3R_2$, $3H_1$, $3H_2$) or both ($3H_3$ -$3H_7$) [16].

As an example, the mentioned mineral with the structure [$Mg_6Fe_2CO_3(OH)_{16}\cdot 4H_2O$] can have a three-layer repeat (3R polytype-pyroaurite) and a two-layer repeat (2H polytype-sjögrenite) [14]. Natural occurred [$Mg_6Al_2(OH)_{16}CO_3 \cdot 4H_2O$] can have $2H_1$- manasseite and $3R_1$-hydrotalcite polytypes. Many synthetic LDHs form 3R structural polytype, for example, [$Zn_2Al(OH)_6Cl\cdot 2H_2O$] [26]. Furthermore, for synthetic LDHs faults in the stacking arrangement can occur, owing to fine intergrowth of rhombohedral with hexagonal polytypes. This fact is based on the equal layer–interlayer topology of the two polytypes. Studies of Pausch et al. [27] and Clause et al. [28] showed the influence of nature and composition of the layer–interlayer bonds and synthesis methodology on the appearance of layer stacking faults.

There are no strong restrictions in the type of balancing anions in the interlayer space. Usually, in naturally-occurring LDHs, the intercalating anions are carbonates. In the synthetic ones, the list of possible anions is wide from inorganic to organic, including biomolecules, pharmaceuticals, vitamins and metal complexes like hexacyanoferrates (II, III) [14, 17, 25, 29]. The change of ratios between cations allows the variations of number and arrangement of charged balancing anions. It makes LDHs a very attractive and interesting object for material scientists in the frame of their possible applications.

Interactions between the anions (guests) and brucite like layers (host) of LDHs are based on the electrostatic interactions and hydrogen bonding between hydroxyl surface groups and the anions. They depend on the ordering of cations and nature of anion. For example, oxoanions can strongly interact with hydroxyls forming dense packing structures.

It is based on the possibility of different rhombohedral and hexahedral stackings to form octahedral, prismatic, and tetrahedral interlayer crystallographic sites, which can ideally accommodate monomeric oxoanions. Optimal hydrogen bonds can be formed, when units are arranged face to face or corner to corner. Carbonates and sulfates form hydrogen bonds with hydroxyls, while nitrates randomly spread in the interlayer space. The intercalation of organic anions is usually accompanied by formation of hydrogen bonds between their anionic groups ($-CO_2^-$, $-SO_3^-$, $-PO_3^{2-}$) and surface hydroxyls, whereas hydrophobic carbon chains are organised out from the hydrophilic layer surface (the lowest energy conformation). Interlayer packing is dependent on charge-size relation of organic anions and the equivalent area of the layer. Thus, optimal packing is formed when the cross-sectional area is similar to the equivalent area of the layer. Besides, guest-guest interactions are determined by the layer charged density. The latter is particularly important for catalytic reactions and in situ polymerization [26].

1.2. Synthesis methodologies of LDHs

LDHs present a class of materials, which can be easily prepared in laboratory conditions. Several general routes of LDH synthesis can be identified:

1. direct synthesis by coprecipitation;
2. ion-exchange of LDH precursor;
3. rehydration of calcined LDH precursor;
4. other routes.

1.2.1. Coprecipitation methodology

It is the most common route for LDH preparation. Its advantage consists of being easily scaled up for synthesising larger amounts of material. This route allows preparation of a variability of LDHs, containing inorganic and organic anions, especially such organic molecules which are very difficult to intercalate by other methods [14, 17].

In general, LDH formation by coprecipitation technique consists in nucleation and growth of M^{2+}/M^{3+} hydroxide layers from an aqueous solution, containing the anion, which will be incorporated in the LDH structure. To ensure simultaneous precipitation of two or even more cations, the synthesis should be carried out with pH control (under supersaturation conditions). For this aim, the choice of pH synthesis should be done according to the following rule: pH should be higher or equal to pH at which the most soluble hydroxide is precipitated [17]. Table 1.2.1 presents the pH values of precipitation of some divalent and trivalent hydroxides.

Table 1.2.1. pH values of precipitation of some divalent and trivalent hydroxides [16].

Cations	**pH at 10^{-2} M**	**pH at 10^{-4} M**	**pH, at which hydroxides re-dissolves**
Zn^{2+}	6.5	8.0	14.0
Cu^{2+}	5.0	6.5	-
Ni^{2+}	7.0	8.5	-
Fe^{2+}	7.5	9.0	-
Co^{2+}	7.5	9.0	-
Mn^{2+}	8.5	10.0	-
Al^{3+}	3.9	8.0	9.0 - 12.0
Cr^{3+}	5.0	9.5	12.5

The mechanism of coprecipitation is based on the condensation of hexaaquo complexes in solution. It gives a possibility for formation of uniformly distributed metal cations of brucite-like layers and solvated interlamellar anions. Without pH control the formation of undesired phases can occur as competing reactions. The choice of optimum pH of synthesis is dependent on the combination and ratio of the cation mixture and nature of the present anion (inorganic or organic). It is stated that formation of single-phased LDH by this technique occurs when the M^{2+}/M^{3+} ratio lies between 2 and 4. If the ratio

will be less than 2, M^{3+} octahedra of hydroxide layer will have a high density and will act as a nuclei for $M(OH)_3$ formation; on the other hand, when the ratio is higher than 4, the formation of $M(OH)_2$ will occur [14, 17].

A (hydro)thermal treatment is usually applied after the precipitation step. Its aim is to increase the crystallinity of obtained material. A conventional aging procedure is performed by heating of LDH suspension at temperatures in the range of 0-100^{0}C during several hours or even days. In the case of some organo-LDHs more elaborated hydrothermal treatments can be applied: heating of the sample in a capsule made from gold or silver or in stainless steel autoclave under high pressure [17].

Benito and collegues [30] prepared three types of LDHs: Mg/Al, Zn/Al, Co/Al intercalated with carbonates by coprecipitation methodology, but instead of the usual thermal treatment, they applied a microwave radiation. Their experiments showed that microwave treatment provides an improvement of the crystallinity of prepared solids and the longer the time of treatment, the more uniform the particle size distribution is. In their subsequent works the range of studied LDHs has been extended, different synthetic methodologies have also been applied, and for all of them the application of microwave thermal treatment improved the properties of LDHs [31].

Coprecipitation can be divided into precipitation at low supersaturation and at high supersaturation. Coprecipitation at low supersaturation is carried out by addition of mixed solutions of metal salts with the chosen ratio into the aqueous solution of desired anion. A second alkali solution is added simultaneously to ensure the maintenance of the necessary pH for precipitation of both metals. pH control can be held by manual detection or by using an automatic titration device. It is also important to take into account the possibility of competing reactions. The desired anion for intercalation should be present in the reaction medium in excess and have a high affinity to the LDH structure. Otherwise, the counter anions can be incorporated, leading to contamination of the material [14]. This condition makes common the use of metal nitrates and chlorides salts as sources of metal cations for the synthesis, because of the low selectivity of LDH to single-charged NO_3^- and Cl^-. On the other hand, special precautions should be taken in the case of carbonates, if they are not the desired anions for intercalation into the LDH structure. This is because LDHs possess a strong affinity to carbonates. Then, to avoid contamination of samples by

carbonates, the synthesis needs to be held under nitrogen or other inert gas atmosphere. By coprecipitation at low supersaturation the following inorganic and organic anions can be intercalated into the LDH structure: CO_3^{2-}, NO_3^-, naphthalene-2,6-disulfonate, tetraphenylporphyrins, anionic azobenzene derivatives, alizarin red S, phenylalanine [17].

The difference of precipitation at high supersaturation with respect to low supersaturation resides in the addition of M^{2+}/M^{3+} mixture into the alkaline solution of the desired anion. The absence of pH control leads to considerable pH variations during synthesis and, as a result, to formation of additional phases of M^{2+}/M^{3+} hydroxides and undesired ratios of metals in the final LDHs. Thus, LDHs prepared by this route, usually have worse crystallinity in comparison to LDHs synthesized by coprecipitation at low supersaturation because in the first case higher number of crystallization nuclei are formed and particle size distribution is also broad (inhomogeneous). However, different bimetallic and multimetallic carbonates containing LDHs can be prepared by this technique, including also LDHs with the following organic anions: caprate, terephthalate, polyaminoacids, dicarboxylates, anti-inflammatory drugs, L-aspartic acid [17].

Wang and collegues [32] prepared organically-modified Mg/Al LDHs with surfactant (sodium dodecylbenzenesulfonate) by a modified coprecipitation technique. It consists of slow addition of metal salts mixture into the solution of surfactant with constant stirring at 50°C, with pH during synthesis kept at 10. The final slurry is then subjected to further stirring during half an hour and then aged in a heater. The analysis of obtained powders showed the successful intercalation of surfactant into the LDH structure. Another advantage of this new technique is the contamination with competitive anions (like carbonates).

Thus, coprecipitation mode allows synthesis of various types of LDHs, including a wide range of inorganic and organic anions. Moreover, coprecipitation at low supersaturation provides a control of the charge density (M^{2+}/M^{3+} ratio) in the LDH final product [14].

1.2.2. Ion-exchange methodology

The ion-exchange methodology is a well-known method, especially for the preparation of organo-LDHs. It is useful when metal cations or anions are unstable in the alkaline solution or the direct reaction between metal ions and guest anion is preferable.

From the thermodynamic point of view, ion-exchange in LDHs is dependent on electrostatic interactions between the positively-charged hydroxide sheets and the exchanging anions and, in a less extent, on the free energy of hydration changes [17]. Thus, the LDH precursor should contain anions with a weak electrostatic interaction with the layers for facilitation of subsequent ion-exchange. On the other hand, the equilibrium constant increases with the decrease of anion radius. Hence, the exchange is favoured for ingoing anions with a high charge density [26]. The easiness of exchange of monovalent anions and divalent anions occurs in the following order [14, 26]:

$$OH^- > F^- > Cl^- > Br^- > NO_3^- > I^-$$

$$CO_3^{2-} > C_{10}H_4N_2O_8S^{2-} > SO_4^{2-}$$

$$HPO_4^{2-}, HAsO_4^{2-} > CrO_4^{2-} > SO_4^{2-} > MoO_4^{2-}$$

Thus, divalent anions possess higher selectivity in comparison to monovalent anions. The strong affinity of LDHs to carbonates demands their preparation in CO_2-free environment as mentioned before [26]. Finally, the most appropriate precursors for ion-exchange reaction contain nitrate and chloride anions. In general, ion exchange is performed by dispersion of LDH precursor in the solution with the excess of the desired anion. The main requirement for the anion to be intercalated is its stability at the exchange pH and also the metals ratio should remain constant during the reaction to provide stability of the hydroxides layers [14, 16].

This methodology allows intercalation of a wide range of anions and molecules: deoxyribonucleic acid [23], Dawson and Finke structures [24], phthalocyanines [25], polyoxometalate anions with Keggin, alkanesulfonates, alkylbenzenesulfonates, ether sulfates [33], mono-and dicarboxylic acids [34, 35], different types of phosphates [36].

1.2.3. Rehydration of calcined LDH precursor methodology

This methodology is based on the so-called "memory effect" [14, 17] and consists of calcination of an LDH precursor in the range of temperatures from 500 to 800^0C. This heat treatment leads to formation of mixed oxides, which rehydrate and reform the LDH structure in the presence of water and the desired anion [14]. It is important to notice, that in this method occurrence of intercalation of competing inorganic anions is prevented, except for carbonates. Hence, the inert atmosphere for reconstruction process is required for preparation of carbonate-free LDHs [17]. The reconstruction process depends on the chemical composition of LDH sheets and calcination temperature. The reconstruction process finishes after 24 hours, if the calcination temperature is at or less 550^0C, 3 days are necessary for reformation after calcination at 750^0C and only partial reconstruction occurs for calcination at 1000^0C [17].

The reconstruction process is based on the topotactic reaction. Investigations of Carlino et al. [37] showed that a slow ramping technique is favourable for the improvement of crystallinity of final rehydrated product. Slow heating helps to prevent fast expulsion of CO_2 and water from the LDH precursor. The thermal behavior of Mg/Al-CO_3 LDH has been described by Stanimirova et al. [26, 38]:

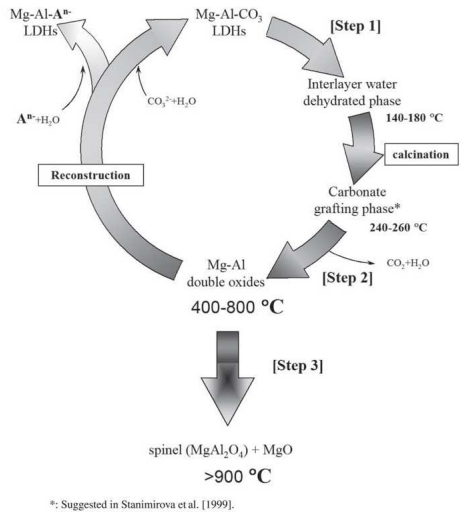

Figure 1.2.3. Scheme of Mg/Al –CO_3 LDH decomposition [26]

According to the presented scheme the following steps of LDH decomposition can be distinguished:

- Loss of interlayer water (up to 250^0C);
- Conversion of LDH into the mixed oxides (250-900^0C);
- Formation of mixture of magnesium oxide and spinel $MgAl_2O_4$ (> 900^0C);

In reality, the processes of 1-3 steps are more complicated than described in this scheme. The loss of water on the first step and conversion on the second step are accompanied by the formation of tetrahedrally coordinated Al. Besides, the location of Al(IV) is uncertain and it disappears on the reconstruction step [26].

This method is usually applied for the incorporation of large guest species: organic chromophores, surfactants, aminoacids and peptides [17]. However, during the reconstruction step some carbonate anions remain in the structure [39- 41]. In the first calcination/rehydration step the change in the crystal symmetry and sorption capacity of LDH can occur [42].

Experiments of Dimotakis and Pinnavaia [14] revealed that the application of a swelling agent (for example, glycerol) promotes the incorporation of organic species through the rehydration mechanism. The final reaction product prepared by this methodology is a well-ordered and single-phase material. Otherwise, without swelling agent, the reaction products are mixed phase.

The advantage of calcination/rehydration methodology is the possibility to intercalate anions different from the ones presented in the LDH precursor, especially when the precursor has strongly held anions on its structure such as carbonate.

1.2.4. Thermal reaction method

Thermal reaction methodology is based on the slow heating reaction between host and guest material to a temperature above the melting point of a guest. By this technique Carlino and collegues have successfully intercalated sebacic and capric acid into the Mg/Al LDHs [43, 44]. For example, capric acid-LDH mixture is heated at a ramping temperature not higher than 1^0C/minute up to 150^0C, that is approximately 120^0C higher than the melting temperature of the acid (31-32^0C). The reaction mixture is held at this temperature during 8 hours and then is cooled down to room temperature (the rate is not higher than 10^0C/minute) and after washing with hot ethanol reaction the product is stored in a CaO desiccator under nitrogen atmosphere [44]. This method performs an interesting alternative to other existing methods.

1.2.5. Urea hydrolysis methodology

The urea hydrolysis methodology is another possible method for LDHs preparation. Urea is a weak Brönsted base (pK_b = 13.8) and highly soluble in water. Hydrolysis of urea occurs in two steps and can be controlled by temperature of the mixture.

1) $CO(NH_2)_2 \rightarrow NH_4(CNO)$ (2)

2) $NH_4(CNO) + 2H_2O \rightarrow 2NH_4^+ + CO_3^{2-}$

The formation of ammonium cyanate is the rate-determining process. Afterwards, fast hydrolysis of this compound to ammonium and carbonate occurs. The pH of reaction is about 9 (temperature dependent) and is suitable for precipitation reaction [17].

Inayat and collegues [45] have successfully synthesized Zn/Al LDHs containing nitrates instead of carbonates in the interlayer gallery by the urea method. The key control parameter is the final pH of the synthesis mixture, which is dependent on synthesis time and initial nitrate/urea ratio. The addition of ammonium nitrate to the reactants leads to formation of pure-phase LDH-NO_3, even independent from synthesis time, caused by the final pH decrease and increase of nitrate/urea molar ratio.

Successful preparation of other types of LDHs by the urea method have also been reported. For example, Hibino and collegues [46] have synthesized Mg/Al-LDHs. Arai et

al. [47] have prepared Co/Al LDHs from aqueous glycerol solutions of cobalt chloride and aluminum chloride by urea hydrolysis under hydrothermal conditions and have studied influence of heating temperature and time and water/glycerol ratio on the particle size of these LDHs, and found, that glycerol addition can affect the rate of urea hydrolysis, which can be correlated with nucleation and/or growth of LDHs. Highly ordered polycrystalline samples of Mg/Ga-CO_3, Co/Ga-CO_3 and Ni/Ga-CO_3 were synthesized by Manohara and colleagues through urea hydrolysis [48].

1.2.6. S*eparate nucleation and aging steps method*

This method can be envisaged as a modification of the coprecipitation methodology. It is known that formation of crystallites occurs in two steps: nucleation and aging. These processes take place simultaneously during the prolonged time process, causing wide and inhomogeneous particle size distributions and shapes after aging step of conventional coprecipitation [15, 17]. To avoid this, the synthesis can be held in a colloid mill (Figure 1.2.6) where the processes of mixing and nucleation take just a short time and are followed by a separate aging process [49]. LDHs prepared by this route have considerably narrower particle size distribution than LDHs prepared by coprecipitation at constant pH.

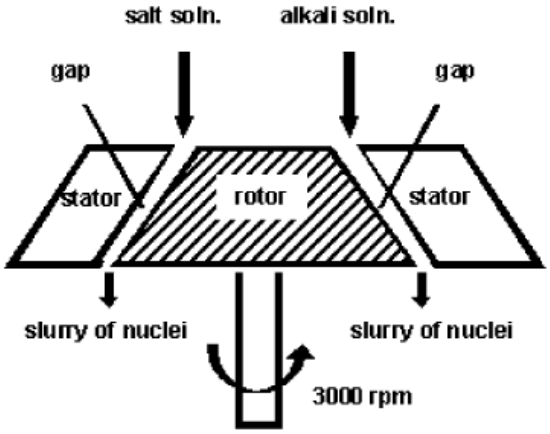

Figure 1.2.6. Scheme of colloid mill [17]

The key of formation of narrow range of crystallite size particles is in the very fast nucleation process in the colloid mill, followed by a separate aging process. The main advantage of this method is the preparation of LDH particles with smaller crystallites,

higher aspect ratio and narrow distribution of crystallite size in comparison to conventional materials [49]. Cho and colleagues [50] have applied this technique for preparation of a composite material based on Ni/Al-LDHs and low density polyethylene in a heated double - roller mixer. Another advantage of this method is that it can be readily scaled-up, which has been successfully applied in China for LDHs preparation.

1.2.7. Reverse microemulsion method

The reverse microemulsions can be applied for control of nucleation and growth of LDHs. In this technique the anionic surfactants are dissolved in organic solvents with the formation of spheroidal reverse micelles, where hydrophobic chains point out to the oil phase. These micelles are necessary for creation of space isolation. After addition of water the micelles will swell with the entrapment of water droplets at the polar cores, which were formed by hydrophilic heads of the surfactants. Hence, under controlled reaction conditions materials will be formed within the limited space. Hu and colleagues [51] have successfully prepared Mg/Al LDH and shown that variations of water content in the recipe lead to formation of LDHs with different sizes. On the other hand, they have also obtained nanometer-sized Mg/Al LDHs platelets in a water-in-oil reverse microemulsion. These reverse microemulsions have been subsequently modified by using triblock copolymers, which resulted in various growth orientations of LDH structures. This can be interesting in the frame of different applications because LDHs prepared by conventional methods usually show a plate-like morphology. The work of Hu and colleagues [52] reveals that the change of synthetic conditions gives the opportunity for preparation of LDHs with new types of morphology like rod-like and belt-like structures. He and colleagues [53] prepared Mg/Al-CO_3 LDHs in a water-in-oil solution (octane-water-sodium dodecyl sulfate) with high surface area and narrow size distribution. Moreover, this method also allows the preparation of LDHs with new morphology, such as loosely stacking fiber-like.

1.2.8. "Chemie douce" method

A "chemie douce" method for LDH preparation was announced by Delmas [17]. Its main aim is to overcome the disadvantages of conventional coprecipitation methodology, such as poor crystallinity and compositional fluctuations of final LDHs. In the first step a high temperature reaction between metal oxides is held. Then γ-oxyhydroxide precursor is prepared by oxidizing hydrolysis using a mixture of NaClO and KOH. In the last stage this precursor is subjected to reduction in the presence of hydrogen peroxide and the salt of desired anion for intercalation into the LDH structure. The list of intercalated anions includes carbonates, metavanadates, sulfates and nitrates among others. The disadvantage of this method is the small range of applicable layer compositions [17].

1.3. Application of LDHs

The features of LDH structure like possibility of preparation of isostructural materials and incorporation of a wide range of inorganic and organic anions and molecules between the hydroxide layers result in application of LDH in fields like catalysis, photochemistry, electrochemistry and biology [54].

1.3.1. Application in catalysis

In 1971 different types of LDHs, containing a variability of metal cations like Zn^{2+}, Mg^{2+}, Ni^{2+}, Mn^{2+}, Cr^{3+}, Al^{3+} and carbonates as interlayer anions, were used as effective supports for Ziegler catalysts in the polymerization of olefins. The maximum of the catalytic activity of polyethylene production was observed for Mg/Mn/Al – CO_3 LDH calcined at 200^0C [54]. LDHs intercalated with polyoxometalate ions can be used for selective adsorption and oxidation catalysis [14, 24].

Dubey [55] synthesized nanosized LDHs within the mesoporous materials (carbon CMK-1), that can be applied as catalysts for aldol and Claisen-Schmidt condensation reactions. Hulea and co-workers studied that W-, V- and Mo-containing LDHs can be successfully used for oxidation of various types of sulfides [56]. LDHs containing Zn/Al-dodecyl sulfate and Mg/Al-terephtalate and their pillared derivatives [57] can be applied in solid base catalysis.

Wang and colleagues [58] suggested a new method of preparation of LiAl mixed oxides from corresponding LDH by separate nucleation and solvothermal aging steps. The synthesized solid catalysts can be effectively applied in Knoevenagel reaction. Studies of application of calcined Li-Al, Mg-Al and Mg-Fe LDHs as catalysts for preparation of biodiesel have been reported by Shumaker et al. [59].

1.3.2. Application in electrochemistry

The interlayer region of LDHs allows intercalation of guest anions with the subsequent application for photochemical reactions [54]. For example, Tagaya and colleagues investigated the photoisomerization of sulfonated indolinespirobenzopyran to

merocyanine in the interlayer space of Mg/Al LDHs and found that this mechanism is irreversible [14]. These materials can originate a class of photoresponsive materials.

Wang et al. [60] prepared a thin film electrode based on Co(3)Al(1)-LDH which performs an economic alternative to the existing thin-film supercapacitor electrodes. Besides, carbon glass electrode modified with Mg-Al-CO_3 LDHs have been successfully applied for registration of bisphenol A in plastic products [61]. $[Co(OH)_2]_{0.41}[Ni(OH)_2]_{0.59}\cdot 0.6H_2O$ LDHs have also been prepared via coprecipitation methodology and due to its high specific capacitance, simple and low-cost preparation technique can become a challenging material in supercapacitor applications [62].

1.3.3. Application of LDHs as adsorbents

LDHs can be successfully applied as adsorbents. The hydrophobic nature and accessibility of the interlayer space of organo-LDHs make them good adsorbent candidates, which can be used for adsorption of pesticides [63-65]. Bruna and co-workers [66] revealed that hydrotalcite like materials based on Mg/Al LDHs can be applied for herbicide removal and that Zn/Al-Cl is a good adsorbent of nitrates from water [67]. Moreover, phosphates can also be successfully adsorbed by calcined LDHs containing various cations compositions: Mg–Al, Zn–Al, Ni–Al, Co–Al, Mg–Fe, Zn–Fe, Ni–Fe, Ca-Fe and Co–Fe [68, 69]. In other words, LDHs also can be widely used in environmental protection.

1.3.4. Application of LDHs in medicine and biology

Another wide field of possible application of LDHs is the area of medicine and biology. LDHs can be used as antacids and stabilizers. Additionally, different biologically-relevant species can be intercalated, including sorbic acid, biocatalysts, vitamins, aminoacids and peptides. Li et al. showed that phenoxymethylpenicillin can be reversibly intercalated into the LDH structure and the final system performs an effective anti-bacterial activity [70]. Moreover, the LDH structure also gives the possibility of carrying anions on its surface, being potential nanocarriers for drugs and genes [23, 71]. Choy et al. [72] showed that LDHs can be employed not only as drug-delivery matrix, but also can increase the efficiency of the delivery process.

1.3.5. Application of LDHs in separation chemistry and corrosion science

The weak interlayer bonds in the LDH structure allow their investigation as possible host structures for different species, including the possibility of supramolecular structures formation. On the other hand, a restricted geometry for the guest species created by the brucite-like hydroxide layers allows LDH application in separated chemistry. The most recent investigations have shown the possibility of using LDHs as nanoreservoirs for corrosion inhibitors and their positive anticorrosion properties [73, 74]. The release of decavanadate species from the Zn/Al hydrotalcite like structure and their properties in the frame of corrosion protection was investigated by Mahajanam et al. [75]. Besides, corrosion inhibitors such as phosphates has been successfully intercalated into the structure of Ca-Fe LDH [76].

The structural versatility of LDHs and the unlimited number of species that can be intercalated into their structure are very attractive points for investigation, from both fundamental and applied scientific perspectives.

Chapter 2. Characterization techniques

2.1. X-ray diffraction (XRD)

During a long period of time information regarding to the molecular and atomic structure of solids has been received from X-ray diffraction analysis and still nowadays this technique is one of the most effective in investigation of structure of new crystalline materials [77, 78].

X-rays are a form of electromagnetic radiation with high energies and short wavelengths on the order of atomic spacings for solids (0.01-1.0 nm) [78]. X-rays can be produced by high-speed electrons accelerated by a high-voltage field that are faced with a metal target.

Diffraction phenomenon occurs when a wave encounters obstacles that are capable to scatter the wave or have spacings comparable to the wavelength. Diffraction can also be considered as a specific phase relationship between two or several waves that have been scattered by obstacles. These phase interactions will depend on the difference of path length and can lead to wave reinforcement (the amplitude of the resultant wave increases) or wave destruction (when the resultant wave after phase relationships has zero amplitude) [78].

X-ray diffraction technique is based on the elastic scattering of X-rays from the electron clouds of the individual atoms in a system. Analysis of the observed diffraction intensity measured as a function of scattered angle and wavelength allows to solve the complete structure of crystalline materials. Bragg's law establishes a relation between several parameters: X-ray wavelength (λ), interatomic spacing (d_{hkl}) and angle of diffraction for constructive interference (θ):

$$n \lambda = 2 d_{hkl} \sin \theta \qquad n \text{ - order of reflection} \quad (3)$$

Bragg's law equation is a necessary, but not sufficient condition for diffraction in real crystals, because it describes diffraction requirements for atoms positioned at unit cell corners and atoms situated at other sites of the unit cell can act as extra-scattering centers and produce out-of-phase scattering at appropriate Bragg's angles. For analysis by common diffraction technique a polycrystalline powder specimen is used. It means the presence of fine and randomly oriented particles that are subjected to monochromatic X-rays radiation. Each powder particle can be considered as a crystal and a large number of

them with different orientations ensure that some particles can be properly orientated and every possible set of crystallographic planes will be available for diffraction. For determination of angles at which diffraction occurs, in the case of powdered samples, a diffractometer is generally used [78, 79].

The definition of position and intensity of diffraction peaks (high intensity peaks result when the Bragg's diffraction equation is satisfied) is used for qualitative identification of the crystalline phase of the material. Using a precise measurement of integrated intensities of diffraction peaks it is possible to make quantitative assessment of the phases that are present in a mixture. Moreover the estimation of peak width allows the determination of crystallite size. Peak width is inversely related to crystal size. In other words, peak width increases with decreasing of crystal particle size [77-80]. For calculation of average crystallite size the Scherrer equation is used:

$$D_{Scherrer} = K \lambda / \beta \cos \theta \qquad (4)$$

where, K-constant (depends on the crystallite shape)

β- integral breadth of the profile

$D_{Scherrer}$- average crystallite size

This equation gives a rough estimation of the broadening caused by crystallite size and hence allows assessment of average size of crystallite. The utilization of XRD technique provides a variety of information about solid material structure: number and ratio of crystalline phases (from the X-ray peak angular positions and intensities); unit cell dimensions (from the peak positions); theoretical density of a solid (if chemical composition is known); average crystallite size (from the peak broadening). Furthermore, lattice strain, texture, coefficients of thermal expansion, atomic coordinates, bond distances and bond angles can be estimated from the detailed analysis of XRD data. Typical XRD pattern of an LDH is demonstrated in Figure 2.1.1.:

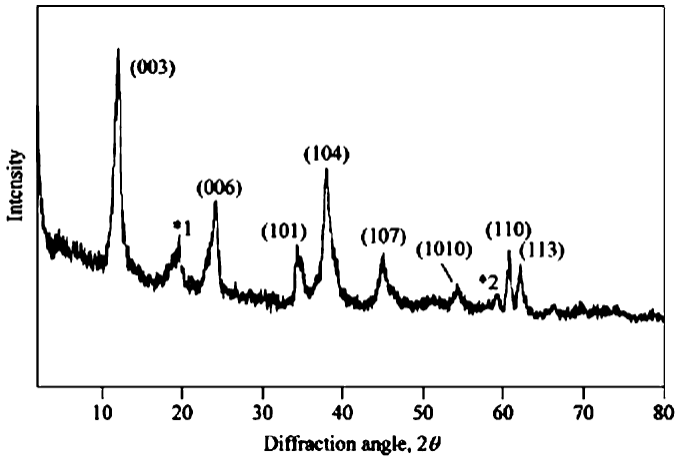

Figure 2.1.1. Diffraction pattern of Mg/Al – CO_3 LDH (peaks ∗1 and ∗2 are due to presence of brucite) [17].

The most representative for the simple analysis of XRD pattern of a single-phase are the following:

- A series of strong basal reflections at low 2θ angles allow the direct determination of the basal plane spacing. The basal spacing is the distance between the adjacent hydroxide layers which is equal to d_{003} in LDHs of 3R polytype. In turn, $3d_{003} = c_0$ is the lattice parameter in a hexagonal setting.
- The position of (110) reflection at high angle (around 60^0 2θ for Cu Kα radiation) allows the estimation of lattice parameter a_0;
- Peak broadening gives information on the crystallinity of the sample [16].

2.2. Fourier-transform Infrared Spectroscopy (FTIR)

Infrared (IR) Spectroscopy is a form of vibrational spectroscopy which describes interaction of electromagnetic radiation with molecular vibrations. IR Spectroscopy is nowadays one of the most popular techniques for identification of molecules. The IR spectrum can be considered as a "fingerprint" that is unique for a molecule. By analysis of IR spectra it is possible to determine presence or absence of different functional groups in organic or inorganic solid, liquid or gas samples. The IR region of electromagnetic spectrum lies between the shortest wavelength of radio waves (wavelength longer than one of few millimeters) and the visible light (approximately 700 nm). Commonly, the vibrational spectroscopy covers a wavenumber range from 200 to 4000 cm^{-1}. It is known that molecules in solids are always in vibration at their equilibrium positions (except for the temperature of absolute zero, -273,15^{0}C). They can be modelled as massless springs connecting nuclei in a molecule. A diatomic molecule vibration by stretching or compressing the bond illustrates the simplest model of a molecule vibration. However, in the case of crystalline solids lattice vibrations are also generated. They refer to the synchronized vibrations of all atoms in the crystal lattice. Such type of vibrations has low frequencies (20-300 cm^{-1}) and can couple with molecular vibrations in this wave range. However, they can be distinguished according to their temperature change sensitivity [77, 81].

One of the major advantages of vibrational techniques is the possibility to analyze all phases of matter and all levels of organization at all relevant timescales: from femtoseconds to months or longer [81, 82]. FTIR is a type of infrared spectroscopy in which the Fourier transform method is used to obtain an infrared spectrum in the whole range of wavenumbers simultaneously. Wavenumber regions and corresponding functional groups are collected in special tables [77, 81].

2.3. Electron Microscopy

Scanning Electron Microscopy (SEM) is one of the main types of electron microscopies. SEM is a versatile technique for microstructural analysis of solids. One of the useful features of this technique is the high resolution in the examination of bulk objects. SEM instruments generally operate in high vacuum and very dry environment for production of a high energy beam of electrons for imaging and analysis. In this technique

the imaging system depends on the specimen that should be sufficiently electrically conductive to ensure that the bulk of incoming electrons goes to ground. Formation of the SEM image is made by a focused electron beam that scans over the surface area of the sample. The most important feature of a SEM is the three-dimensional appearance of the images due to large depth of the field that provides additional information of the surface of a wide range of materials: heterogeneous organic and inorganic specimen on micrometer to nanometer scale. In addition, SEM allows obtaining chemical information by using the X-ray energy dispersive (EDS) spectrometer [77, 83].

2.4. Dynamic light scattering (DLS) and Zeta potential

During the last decades light scattering has been widely used as a tool in many branches of materials science, including both experimental and theoretical aspects. When a light beam illuminates a piece of matter with a dielectric constant different from unity, light is absorbed, scattered, or both, depending on the wavelength of light and the optical properties of the material. Scattering is observed when light interacts with the electrons bound the material. According to the fluctuation theory of light scattering the intensity of scattered light can be calculated from the mean-square fluctuations in density and concentration. They can be determined from the isothermal compressibility and the concentration-dependence of the osmotic pressure. Thus, the intensity of the light is obtained without consideration of the molecular structure of the medium in detail and this approach has become a base of light scattering theory. DLS is based on light scattering dependency from the nature and properties of the material [84, 85]. The particle size measured in DLS is a diameter of the sphere that diffuses at the same velocity as the particle being measured. The size is determined by measurement of the Brownian motion of the particles in the specimen. The particles in the liquid move randomly and their speed of movement is used for determination of particle size.

Most of liquids contain cations and anions. When charged species are suspended in liquid, ions of opposite charge will be attracted to the surface of the suspended particle. It leads to formation of ions layers. The first consists of ions that are strongly bound to a particle. The second is a diffuse layer of other ions that are loosely bound the specie. Within this boundary in the diffuse layer all ions will move together with the particle when it moves in the liquid, but other ions will stay like they are, the last boundary is called the

slipping plane. Potential at the slipping plane between the particle surface and the dispersing liquid (varies according to the distance from the particle surface) is called Zeta potential. It can be measured by combination of techniques: Electrophoresis and Laser Dopler Velocimetry (Laser Dopler Electrophoresis) [86].

2.5. Inductively Coupled Plasma (ICP) Spectroscopy

Nowadays, ICP is one of the most effective source for emission spectroscopy. Initially, the stream of argon becomes conducting by a pilot electric spark, arc or Tesla discharge. Then a radio frequency field (27 to 40 MHz) creates a magnetic field inside the argon flow and spectrally intense plasma at a temperature of 9000 to 10 000K is obtained in the annulus of an ICP discharge [82].

ICP spectroscopy allows simultaneous determination of about 70 elements in the sample during several minutes. Detection limits are generally in the range 0.02–2 ppb. This technique is used for various applications like determination of trace impurities and ultratrace elements in raw materials, intermediates and final products, for detection of radionuclides and isotopic traces. Samples for analysis are usually applied in the liquid form (solids are quantitatively dissolved). 50 mg of the material is dissolved in 50 ml of total volume of solution. Smaller sample masses can be unrepresentative, especially, if the material is inhomogeneous. It is desirable to reduce the total amount of solids as much as possible (but in the range of the detection limits), because the sampling orifice (1 mm of diameter) can be clogged if the solutions contain more than 1000 ppm of total dissolved solids introduced into plasma. The limitations of this technique are the following: concentration of measured solutions should be less than 1000 ppm; organic solutions require addition of oxygen into plasma or additional pretreatment of the specimen to avoid the clogging of the sampling orifice with elemental carbon; the optimization of sensivity and accuracy demands application of high purity reagents and extreme caution to avoid contamination and losses. Moreover, ICP spectroscopy does not allow detection of oxidation states of compounds. However, the main restriction is connected with the necessity of analites to have ionization potential less than of argon (15.8 eV), hence ICP spectroscopy does not allow detection of the following elements: hydrogen, carbon, nitrogen, oxygen, fluorine, chlorine, bromine, mercury, sulphur, rare gases (neon, krypton, xenon) [82, 87, 88].

2.6. Thermal Analysis

Thermogravimetric analysis (TGA/TG) is an experimental technique, is based on the measurement of mass changes with temperature. The procedure of the analysis can be divided in the dynamic measurement (when the sample is heated at the constant heating rate) and isothermal measurement (when the specimen is held at constant temperature). The measurement is performed using thermobalances. This equipment is a combination of suitable electronic microbalance with a furnace, a temperature programmer and a computer for control. This system allows simultaneous weighing, heating or cooling of the sample in a controlled manner and the values of mass, temperature and time can be monitored. The balance should be located in an enclosed system (for temperature, pressure and environmental nature control). The atmosphere used in the TG experiment also influences the final results, because it can be inert, reactive or oxidising [89-91]. TG measurements are corrected for the effect of buoyancy (because of the changes in density of gas with the evolution of temperature) by performing a blank measurement. In the blank experiment the same temperature program and crucible without the sample are used. The resulting blank curve (called baseline) is then subtracted from the sample measurement curve. In some instruments, a 'standard' baseline is automatically subtracted from all measurements. Usually for performing of TG measurements alumina crucibles are used (because of the possibility for heating up to 1600^0C). The results of TG measurements are usually displayed as a TG curve in which mass, or percent mass, is plotted against temperature and/or time. The use of first derivative of the TG curve with respect to temperature or time can be a complementary presentation of the measurements (DTG curve). There are some additional curves that can be useful for results characterization: DTA curve (shows exothermic or endothermic events); EGA (evolved gas analysis) –FTIR or mass spectrometry measurements of evolved gases [89].

Mass losses can occur by different ways, when the material reacts with the surrounding atmosphere. It produces steps in the TG curve or peaks in the DTG curve. It is necessary to take into account several processes, that may cause mass loss: evaporation of volatile constituents, drying, desorption and adsorption of gases, moisture and other volatile substances, loss of water or crystallisation; oxidation of metals and oxidative decomposition of organic substances in air or oxygen, thermal decomposition in an inert atmosphere with the formation of gaseous products (in the case of organic substances, this

process is known as pyrolysis or carbonisation), heterogeneous chemical reactions. In the case of ferromagnetic materials: possibility of magnetic properties changes. Application of TG can be slightly restricted, because not all thermal events are accompanied with mass losses. However, for desorption, decomposition and oxidation processes TGA can provide important information. This knowledge can be applied for definition of conditions of explosive materials storage, definition of shelf-life of drugs, the conditions of drying tobacco and other crops [89, 90].

Chapter 3. Experimental part

3.1. Materials

All the chemicals were received from Aldrich, Fluka and Riedel-de Häen with the content of ground substance > 98% and were used as obtained. All solutions were prepared using boiled distilled water and synthesis by *coprecipitation methodology* was held in nitrogen atmosphere to prevent contamination with carbonate. The variety of prepared LDHs and synthetic methodologies are adopted in Table 3.1.1.

Table 3.1.1. Composition and synthesis methodologies of LDHs adopted in this work.

Parameters		
Cations	Divalent (M^{2+})	Trivalent (M^{3+})
	Zn^{2+}; Mg^{2+}	Al^{3+}; Cr^{3+}
Cations ratio (M^{2+}/M^{3+})	2:1; 3:1	
Intercalating anions	NO_3^-; MoO_4^{2-}; VO_3^-; MBT^-; HPO_4^{2-}	
Synthetic routes	Coprecipitation; calcination-rehydration	

3.2. Layered double hydroxides: synthesis methodologies

In the present work two synthesis routes were used:

- Coprecipitation/(an)ion-exchange for intercalation of corrosion inhibitors [73, 74];
- Calcination – rehydration [14, 17, 26];

3.2.1. Synthesis by coprecipitation/(an)ion-exchange

50 ml of nitrates mixture of divalent (M^{2+}) and trivalent (M^{3+}) metal cations with certain proportions (Table 31.1) were added dropwise to a 100 ml solution of $NaNO_3$ (the concentration of $NaNO_3$ is three times greater than the concentration of M^{2+} nitrate solution) under vigorous stirring at room temperature. The value of solution pH was monitored using pH-meter and was kept constant through continuous addition of 2M NaOH solution (the level of pH depends on the content of cations mixture and pH of precipitation of both cations, the range of pH values varies from 7 to 10). On the next stage LDH slurry was subjected to thermal (aging) treatment in water bath to promote crystallization of LDHs (interval of time and temperature will be discussed thereafter). After the thermal treatment step, the aged LDH suspension was cooled down to room temperature and was subjected to centrifugation at 10000 r.p.m. (Centrifuge Sigma

Sartorius 2-16P) during three minutes (these conditions allow all LDH particles to settle). Afterwards, LDHs was washed with boiled distilled water and was centrifuged two times. At this point LDH-NO_3 precursor is ready for intercalation of corrosion inhibiting anions.

Ion-exchange reaction. LDH-NO_3 precursor was immersed in 0.1M solution of corrosion inhibitor (with certain values of pH: for MoO_4^{2-}- 9.2; VO_x^{n-}- 8.4; MBT^--10.0; $H_xPO_4^{n-}$- 7.0) under constant stirring for 24 hours. After centrifugation/washing procedures (two times) ion-exchange process was repeated. The prepared LDH-inhibitor was dried in oven at 60^0C and was milled using mortar and pestle.

3.2.2. Synthesis by calcination-rehydration methodology

In present work synthetic hydrotalcite (refered hereafter as SH with formula - $[Mg_6Al_2(OH)_{16}CO_3 \cdot 4H_2O]$) in powder form was used as precursor in the calcination – rehydration methodology. The conditions of the calcination process are the following: 650 ^{0}C for 2 hours with slow heating (~ 1 ^{0}C min^{-1}) and cooling down to room temperature (~ 10 ^{0}C min^{-1}) ramping techniques. The rehydration consists of immersion of calcined sample in 0.1M solution of corrosion inhibitor (with the same values of pH that have been used for ion-exchange methodology) and includes two steps: the first lasts for 48 hours, after which centrifugation and washing procedures (two times) were performing, the second rehydration procedure lasts 24 hours. Then, the prepared LDHs were centrifuged (Centrifuge Sigma Sartorius 2-16P) and washed two times, were dried at 60^0C and were milled in the mortar.

3.2.3. Post-treatment of LDH samples

For the production of fine LDH powders ball milling or lyophilisation procedures were used. For ball milling of prepared LDHs Retsch PM 400 was used (200 r.p.m., 2 hours, using zirconia spheres of different sizes within a Teflon-made container). For lyophilization LABCONCO Freeze dry system/Lyph Lock 4.5 was applied. Samples to be lyophilised were first placed in a freezer for 24h, followed by 48 h in the lyophilizer for complete drying of the samples.

3.3. Characterization of LDHs

The resulting particles were characterized by X-ray diffraction (XRD) (1) and Fourier-transform infrared (FTIR) spectroscopy (2). Morphology was investigated by scanning electron microscopy (SEM) (3). For investigation of LDHs particle size and estimation of colloidal stability dynamic light scattering (DLS) (4) was used. Estimation of chemical composition of mentioned types of LDH was made by Inductively Coupled Plasma (ICP) Spectroscopy (5) For exploration of thermal behavior of LDHs thermogravimetric analysis (TG) was performed (6).

1) XRD analysis was made using Philips X'Pert difractometer (Ni-filtered Cu Kα radiation, tube power 40 kV, 50 mA, X'celerator detector) at room-temperature.
2) FTIR measurements were performed on FTIR- IF55 Bruker Germany, ATR-Golden Gate Specac 128 scans Resolution 4 Detector DTGS/ KBr with the range of wavenumbers 4000 – 400 cm^{-1}.
3) SEM measurements were performed using Hitachi S4100 with electron beam energy of 25 keV and Hitachi SU-70 scanning electron microscopies (SEM) coupled with energy dispersive spectroscopy (EDS). LDHs for measurements were dispersed in ethanol or water (for MBT- containing LDHs) using ultrasound and after were placed on the H-terminated silica on the holder. Finally, samples were covered with carbon.
4) DLS measurements (determination of particle size distribution and zeta-potential measurements) were performed on Malvern ZetaSizer Nanoseries. Preparation of the samples for measurement was carried out according to the specifications [86]. Aqueous suspensions of LDH were sonicated in the ultrasound bath for 5 minutes before the measurements.
5) For ICP analysis an ICP Jobin Yvon Activa-M was used. The LDH powder was dissolved in 0.1M hydrochloric acid and diluted with deionised water. The pH of prepared solutions was around 2 - 2.5 [88].
6) TG/DTA measurements were held using Setaram with Labsys model. The sample was heated from 50 to 1000 ^{0}C at a rate 10 ^{0}C/min. in the argon atmosphere in alumina crucible [91].

.

Chapter 4. Results and discussion

Part I. Preparation of nanoreservoirs by coprecipitation methodology

4.1. Synthesis of LDH precursor

LDH precursor with nitrate anions between the layers (LDH-NO_3) was prepared in the first step by the coprecipitation methodology for subsequent intercalation of corrosion inhibitors. One of the most studied precursor compositions of di- and trivalent cations contains Zn and Al in the ratio 2:1. The synthetic conditions of this LDH precursor need to be optimized aiming at LDHs with appropriate properties for their further incorporation as nanoreservoirs of corrosion inhibitors in anticorrosion coatings. The synthesized nanoreservoirs should possess uniform particle size distribution and colloidal properties optimal for their introduction into the coatings. Therefore, the first part of the work was devoted to the investigation of effect of synthesis conditions on the properties of LDH samples. The following parameters that could potentially influence particle size and colloidal properties of LDHs were studied:

- Thermal (aging) treatment;
- Presence of negatively- and positively-charged surfactant in the reaction medium;
- Synthesis temperature;
- pH;
- Drying process;

Table 4.1.1. Investigation of the effect of synthesis conditions on colloidal and structural properties of Zn(2)Al(1)-NO_3 LDHs.

	Synthesis Temperature, ^{0}C	pH	Presence of surfactant	Thermal treatment	Method of drying	Average particle size, nm	Zeta-potential, mV	XRD
Zn(2) Al(1)-NO_3	Room temperature*	10	-	-	lyophilizer	366	+34.2	Two LDH phases
	Room temperature*	10	-	60^{0}C, 20 h	lyophilizer	627	+39.9	Single-phase crystalline structure
	Room temperature*	10	-	90^{0}C, 12 h	lyophilizer	395	+39.7	Single-phase crystalline structure
	Room temperature*	10	-	100^{0}C, 4 h	oven	638	+41.2	Single-phase crystalline structure
	50.5 ± 1	10	-	100^{0}C, 4 h	lyophilizer oven	553; 864	+47.1; +44.9	Single-phase crystalline structure
	0	10	-	100^{0}C, 4 h	lyophilizer oven	5810; 5220	+30.7; +35.8	Single-phase crystalline structure
	Room temperature*	10	Hexadecyltrimethylammonium bromide	100^{0}C, 4 h	lyophilizer oven	621; 2650	+37.9; +39.2	Single-phase crystalline structure
	Room temperature*	10	Sodium *p*-toluene sulfonate	100^{0}C, 4 h	lyophilizer oven	1145; 708	+35.9; +32.4	Single-phase crystalline structure
	Room temperature*	7	-	100^{0}C, 4 h	oven	611	+33.0	Single-phase crystalline structure
	Room temperature*	4	-	100^{0}C, 4 h	oven	300	+33.6	Single-phase structure with less crystallinity

* Room Temperature: 20-25^{0}C

Figure 4.1.1. shows particle size distribution and XRD patterns obtained for Zn(2)Al(1)-NO_3 LDHs subjected to different thermal treatments. Typically, the XRD pattern obtained for LDH-NO_3 indicates a single-phase structure, with well-defined peaks at $2\Theta \approx 10$, 20 and 30°. These signals correspond to reflection by planes (003), (006), and (009). In addition, results of ICP measurements showed that Zn:Al ratio in the Zn(2)Al(1)-NO_3 is 1.78: 1 which is approximate to the theoretical value 2:1.

According to the results presented in Figure 4.1.1 and Table 4.1.1, the aging time is more detrimental (longer times=larger particles) than the aging temperature. A considerable number of particles smaller than 1 µm was detected in LDH samples where the thermal treatment was not performed or it was shorter (12 h/90^{0}C or 4 h/100^{0}C as compared to 20 h/60^{0}C). However, the absence of thermal treatment process results in preparation of LDHs particles with lower crystallinity (Figure 4.1.1 b). Therefore, a thermal treatment with higher temperatures and shorter aging times (100^{0}C/4 h.) was chosen for further preparation of Zn(2)Al(1)-NO_3 LDH precursor.

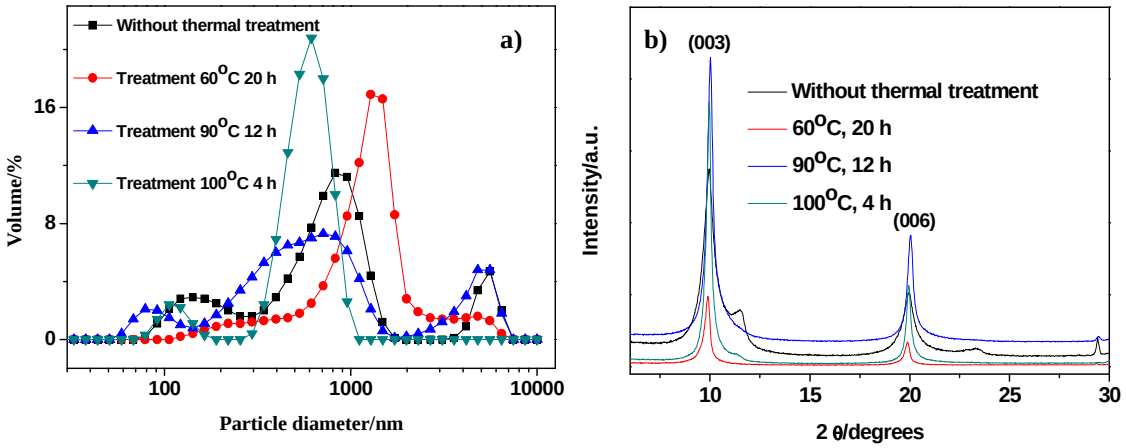

Figure 4.1.1. Particle size distribution (a) and corresponding XRD pattern (b) of Zn(2)Al(1)-NO_3 as a function of temperature and time of thermal treatment.

Figure 4.1.2 depicts particle size distribution and XRD patterns obtained for Zn(2)Al(1)-NO_3 synthesised in the presence of different surfactants during the coprecipitation step, different temperatures, pH and subjected to different drying processes.

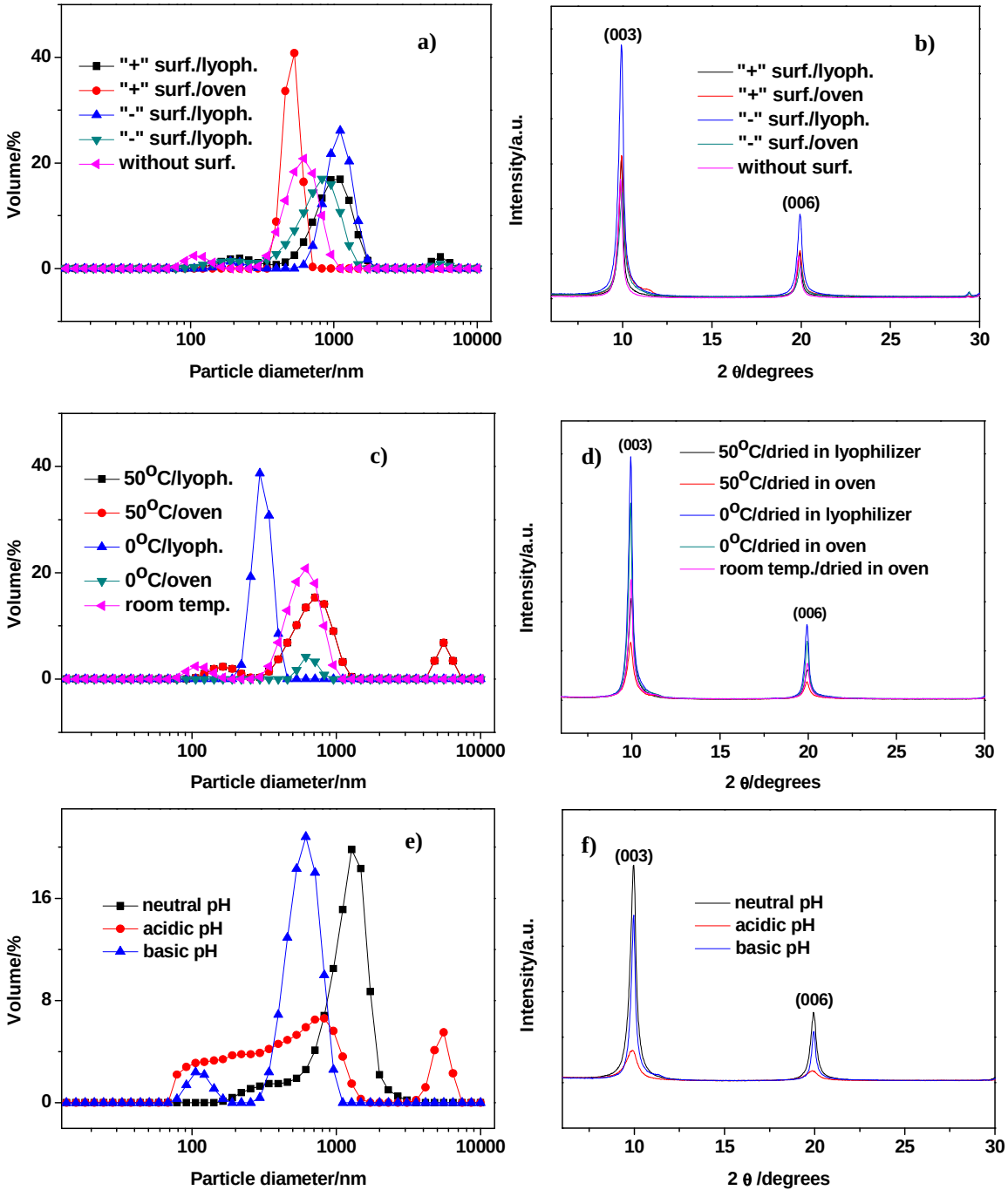

Figure 4.1.2. Influence of surfactants ("+" - Hexadecyltrimethylammonium bromide; "-" - Sodium p-toluene sulfonate and drying process (a, b); synthesis temperature and type of drying process (c, d); pH (e, f) on particle size distribution and structure of Zn(2)Al(1)-NO_3.

The presence of cationic (hexadecyltrimethylammonium bromide) and anionic (sodium *p*-toluene sulfonate) surfactants and temperature/pH of the reaction medium do not decrease the agglomeration of LDH particles (Figure 4.1.2 a, c, e). Synthesis at low temperature (0^0C) favours to formation of the particles with size distribution in the range lower than 1 μm, while high temperature synthesis (50^0C) leads to broader distribution of particle sizes. On the other hand, particle size distributions of Zn(2)Al(1)-NO_3 LDHs prepared at different pH conditions do not differ in a big extent. The formation of crystallites occurs in two steps: nucleation and aging. While the crystallites are subjected to aging in its mother liquor, they can be involved in several processes like crystal growth, agglomeration, breakage [17]. The obtained results imply that the agglomeration is a result of the growth of LDH particles in the presence of a relatively large amount of reactants and due to the occurrence of processes such as Ostwald ripening. This phenomenon consists in the growth of large particles at the expense of smaller ones (it can occur both in crystals and emulsions) [92]. Ostwald ripening can be connected with higher surface energy of smaller particles (higher total Gibbs energy) in comparison to larger particles and hence a tendency to dissolution of smaller particles and their re-deposition on the surface of larger particles. Additionally, the presence of several maxima in the particle size distribution is an indication of broad size distributions, and is related to different times of nucleation and growth for different particles that leads to appearance of particles with different sizes and is intrinsic to the preparation of the LDHs used in this work.

For morphological characterization of Zn(2)Al(1)-NO_3 SEM measurements were also performed (Figure 4.1.3.). The SEM images reveal that LDH particles have a plate-like morphology. Moreover, there is tendency for formation of sub-micrometer sized agglomerates, which is in agreement with particle size measurements shown before.

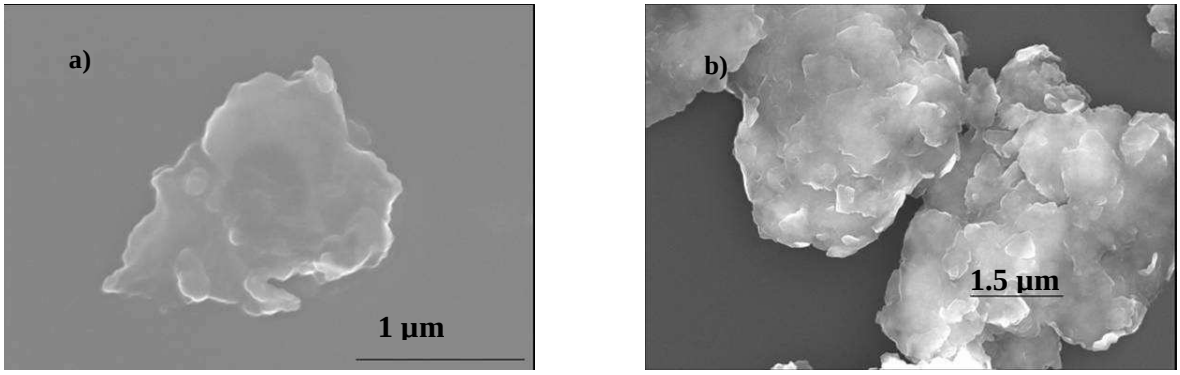

Figure 4.1.3. SEM images of Zn(2)Al(1)-NO_3 prepared by regular synthesis (coprecipitation) at room temperature and dried in oven (a); regular synthesis by coprecipitation at room temperature and dried in oven and afterwards ball milled (b).

SEM images of Zn(2)Al(1)-NO_3 precursor demonstrate the plate like morphology of the LDH particles, but the particle size obtained from ZetaSizer Nanoseries assumes spherical particles [86]. Hence, it is necessary to make some corrections. As an example, Zn(2)Al(1)-NO_3 LDH sample dried in oven will be taken (conditions of thermal treatment is 100^0C, 4 h). The measured diameter by DLS is a hydrodynamic diameter. The hydrodynamic diameter of the platelets can be estimated assuming the oblate spheroid shape using the following formula [93]:

$$D_H = a \frac{(1 - \lambda^2)^{0.5}}{\cos^{-1} \lambda}$$

a, b- longer and shorter spheroid axis length;

$\lambda = b/a$

The value *a* is taken from SEM images (for one of the agglomerates) and *b*-value of LDH thickness – from the literature [74], because SEM technique does not allow estimation of this parameter:

a = 655 nm, b= 30 (this value is in the range of 20-40 nm)

$D_{H\ measured}$ = 638 nm and $D_{H\ spheroid\ calculated}$ = 653 nm. It means, that calculated diameter is slightly higher than the measured by DLS and accounts for the deviation of particle shape from spherical shape. However, even with these approximation, DLS can be used to compare different samples of LDHs.

Figure 4.1.4. presents the dependency of Zn(2)Al(1)-NO_3 particle size distribution on the drying and post-treatment of LDH powders. The particle size distribution shows the

presence of several peaks as mentioned above, which seems to be a feature of the synthesis methodology used in this work. However, the drying process also affects the particle size distribution. The use of lyophilization as drying process leads to a narrower particle size distribution, with respect to drying in oven at 60 ºC. However, the application of ball milling procedures (200 r.p.m., 2 hours) leads to smaller particles due to destruction of micrometer-sized agglomerates. Thus, drying in oven with subsequent ball milling was used for purpose of time economy and energy, especially when LDHs were prepared in large amounts (2 g vs. 10-50 g).

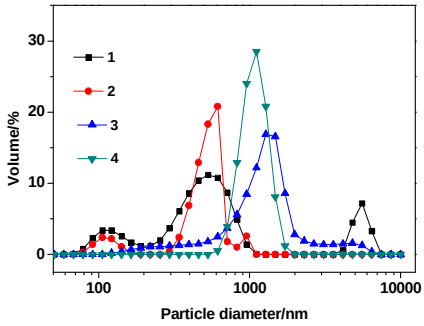

Figure 4.1.4. Dependency of particle size distribution from type of drying Zn(2)Al(1)-NO_3 sample (1-wet; 2-dried in lyophilizer; 3-dried in oven; 4-dried in oven and ball milled.

Another route adopted to decrease particle size was based on application of an ultrasound methodology during the coprecipitation step. A vibrating cell (T=20 ºC, frequency: 20 kHz) was used to control the particle size, with the LDH precursor prepared in the vibrating cell. Then, part of the obtained slurry was subjected to regular thermal treatment in water bath (100 ^{0}C, 4 h) whereas the other part was continuously exposed to ultrasound during 4 hours. The results of particle size distribution for Zn(2)Al(1)-NO_3 LDHs synthesized by these two techniques are depicted in Figure 4.1.5.

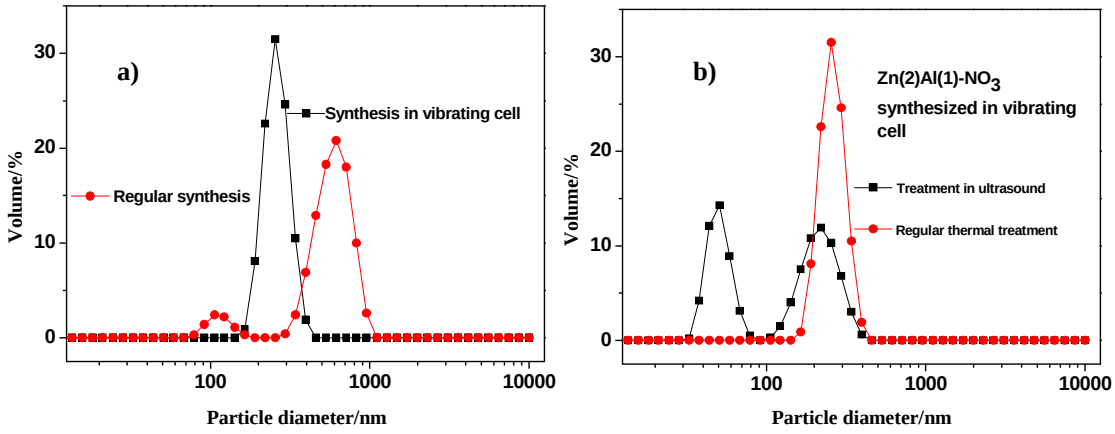

Figure 4.1.5. Particle size distribution of Zn(2)Al(1)-NO_3 prepared by regular coprecipitation and coprecipitation in ultrasound (a) with subsequent regular thermal treatment and treatment in ultrasound (b).

These experiments reveal that utilization of ultrasound during LDH synthesis by coprecipitation methodology leads to narrower particle size distribution in comparison to regular route. Subsequent use of ultrasound instead of regular thermal treatment leads to appearance of two maxima of distribution, both with smaller particle size.

Thus for preparation of LDH precursor by coprecipitation methodology on the base of Zn(2)-Al(1)-NO_3 the following synthesis conditions were applied:

- Synthesis pH ≈ 10;
- Thermal treatment (aging) for 4 hours at 100^0C in the water bath;
- Drying in oven at 60^0C with subsequent ball milling;

For preparation of LDH precursor with narrower particle size distribution the regular coprecipitation methodology can be modified using ultrasound treatment.

Once several experimental factors were studied and optimised for Zn-Al-NO_3 LDHs, other types of LDH precursors were synthesized by coprecipitation using Mg/Al cation mixture with cations ratio 2:1 and 3:1 and nitrates as intercalated anions (Mg(x)Al(1)-NO_3). The structure, morphology and distribution of particles of the prepared samples are depicted in Figure 4.1.6. The average particle size and zeta potential of MgAl-NO_3 LDHs are presented in Table 4.1.2.

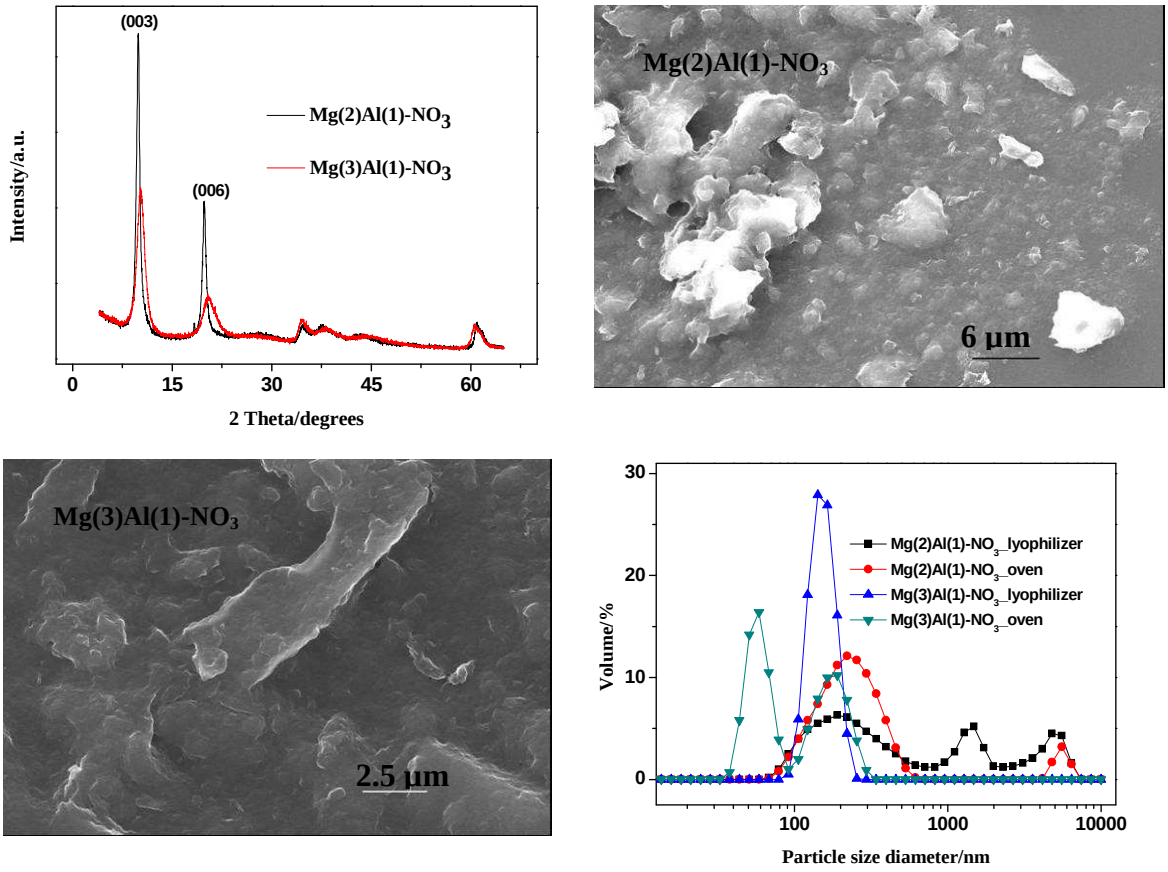

Figure 4.1.6. XRD pattern, SEM images and particle size distribution for Mg(x)Al(1)-NO_3; x = 2,3.

The obtained results show that both types of LDHs precursors based on Mg/Al mixture of cations were prepared successfully. XRD patterns show reflections assigned to LDH phase and the position of peaks is consistent with the presence of nitrates (see detailed description below). In addition, the obtained LDHs show a plate-like morphology as in the case of Zn-Al LDHs. The maximum of particle size distribution and zeta-potential reveal that these systems are stable in water and particle size distribution of LDHs is not significantly affected by the drying procedures.

Table 4.1.2. Colloidal properties of Mg(x)Al(1)-NO_3 LDHs.

LDH	Maxima of particle size distribution, nm	Zeta potential, mV
Mg(2)Al(1)-NO_3 dried in lyophilizer	190.00; 1480.00; 4800.00	+34.80
Mg(2)Al(1)-NO_3 dried in oven	220.00; 5560.00	+37.50
Mg(3)Al(1)-NO_3 dried in lyophilizer	142.00	+37.10
Mg(3)Al(1)-NO_3 dried in oven	58.80; 190.00	+29.60

The third type of LDH-precursor synthesized by coprecipitation in this work is based on Zn/Cr(III) mixture with cations ratio 2:1. The structural, morphological characterization and colloidal properties of this LDHs are presented in Figure 4.1.7 and Table 4.1.3.

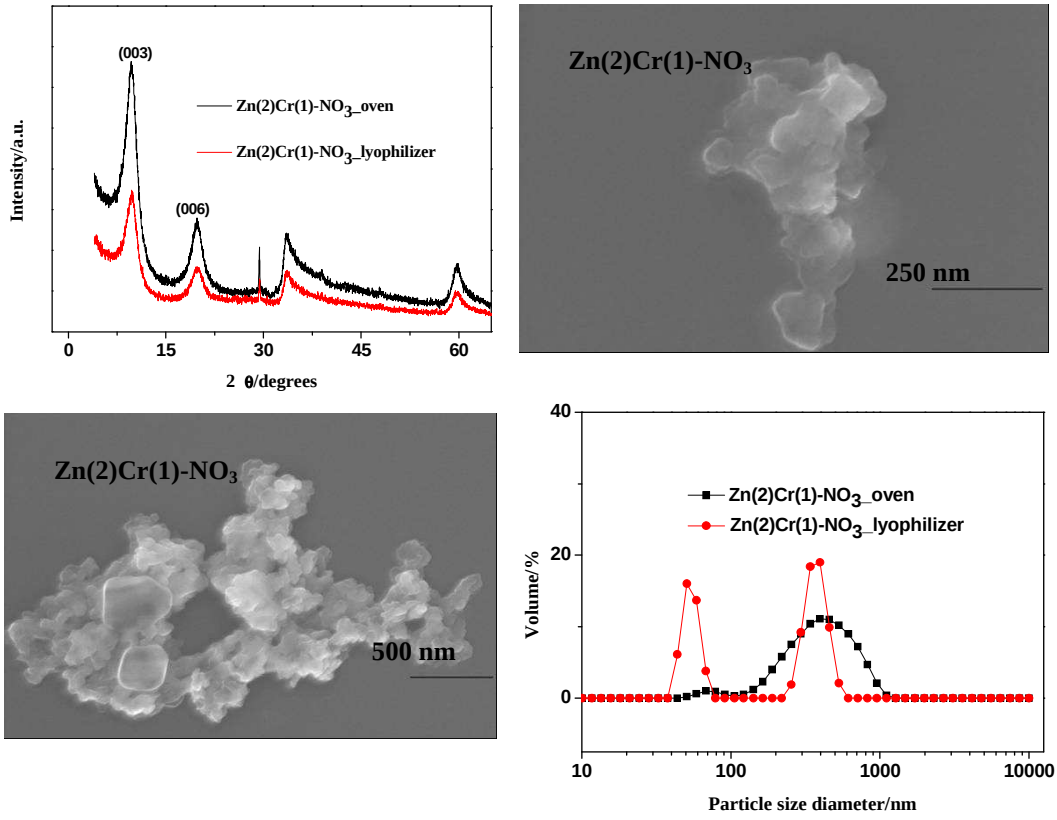

Figure 4.1.7. XRD pattern, SEM images and particle size distribution of Zn(2)Cr(1)-NO_3.

Table 4.1.3. Colloidal properties of Zn(2)Cr(1)-NO_3 LDHs.

LDH	Maxima of particle size distribution, nm	Zeta potential, mV
Zn(2)Cr(1)-NO_3 dried in lyophilizer	50.70; 396.00*	+15.60
Zn(2)Cr(1)-NO_3 dried in oven	68.10; 397.00*	+15.60

***** estimation is complicated, because of colloidal instability of the system

The results show that Zn(2)Cr(1)-NO_3 LDH suspension is unstable in water, which makes the particle size distribution obtained by DLS quite doubtful, since there may be particles that sediment rapidly and are not accounted for. In addition, the difference between maxima of particle size of the samples dried in oven and in lyophilizer seems not to be significant, but the broadening of particle size distribution is much more evident in the case of samples dried in the oven.

Table 4.1.4. describes the parameters obtained from analysis of the XRD patterns using Scherrer's and Bragg's equations (equations 3, 4).

Table 4.1.4. Parameters calculated using diffractograms of LDHs precursors.

Composition	Average crystallite size, nm	Basal spacing, nm
Zn(2)Al(1)-NO_3 regular synthesis	44.80	0.89
Zn(2)Al(1)-NO_3 synthesis with ultrasound	10.60	0.89
Mg(2)Al(1)-NO_3	15.80	0.89
Mg(3)Al(1)-NO_3	4.10	0.86
Zn(2)Cr(1)-NO_3	4.00	0.90

All types of LDH precursors as nanoreservoirs for corrosion inhibitors were successfully prepared by coprecipitation methodology. The formation of LDH structure was confirmed by well-defined peaks in the diffractograms typically found at $2\Theta \approx 10$, 20 and 30°. for all types of prepared LDHs-NO_3 corresponding to reflection by planes (003), (006) and (009). Furthermore, the results depicted in Table 4.1.4. show that the values of average crystallite size and basal spacing depend on the type of precursor.

Using the data of interlayer spacing d_{basal} it is possible to assume the variant of the interlayer anion arrangement: horizontally, vertically or tilted [14]. The gallery height in LDHs can be assessed by subtracting the thickness of brucite layers (estimated to be 0.48 nm), applying the following equation: $d_{basal} = 0.48 + r_{anion}$ *(nm);* r_{anion} – Van der Waals radii of appropriate atoms of the anion; d_{basal} is determined from XRD measurements [16, 94]. The diameter of NO_3^- is 0.38 nm, hence using the mentioned equation the value of gallery height (theoretical) should be 0.86 nm. The presented values of basal spacing for Zn(2)Al(1)-NO_3 in Table 4.1.4 are in agreement with the expected values.

The average crystallite size of Zn(2)Al(1)-NO_3 LDH prepared in ultrasound conditions was found to be lower than for the sample produced by conventional synthesis.

Another important aspect is the comparison between crystallite average size (Table 4.1.4.) and the results from DLS measurements. It is important to notice that the values reported in Table 4.1.4. represent the average size of crystallites, while DLS measurements yield the average size of particles. These values are different because particle contains many crystallites and one of the features of LDHs particles is their strong tendency to agglomerate (the last is confirmed by values of Zeta potential). LDHs can also be made of crystallite domains which contain primary and secondary particles (that were formed at different time during coprecipitation process and had different time for growth of the particles).

Synthesis parameters that influence the colloidal properties of LDH particles were studied in detail for Zn(2)Al(1)-NO_3 and subsequently applied for other types of LDH precursors (Mg(x)Al(1)-NO_3, x = 2, 3 and Zn(2)Cr(1)-NO_3).

4.2. Intercalation of corrosion inhibitors in nanoreservoirs

LDH nanoreservoirs were loaded with corrosion inhibitors by ion-exchange reaction (description in the Experimental part). According to Table 4.1.1 the following types of corrosion inhibitors were used: MoO_4^{2-} (Na_2MoO_4); VO_3^- ($NaVO_3$); MBT^- (2-mercaptobenzothiazole); HPO_4^{2-} (Na_2HPO_4).

Crystal structure and phase content of the synthesized samples loaded with corrosion inhibitors, their crystallinity and level of completeness of ion-exchange reaction were characterized by XRD and FTIR methods. Figure 4.2.1. presents the structural characterization results obtained for LDHs loaded with different corrosion inhibitors. The samples are based on Zn(2)Al(1)-NO_3 prepared by regular methodology (a, b) and by coprecipitation methodology in ultrasound (c), using the same conditions that are described in the Experimental part. Morphological characterization of synthesized nanoreservoirs is depicted in the Figure 4.2.2. and Table 4.2.1 presents the results obtained from analysis of XRD patterns.

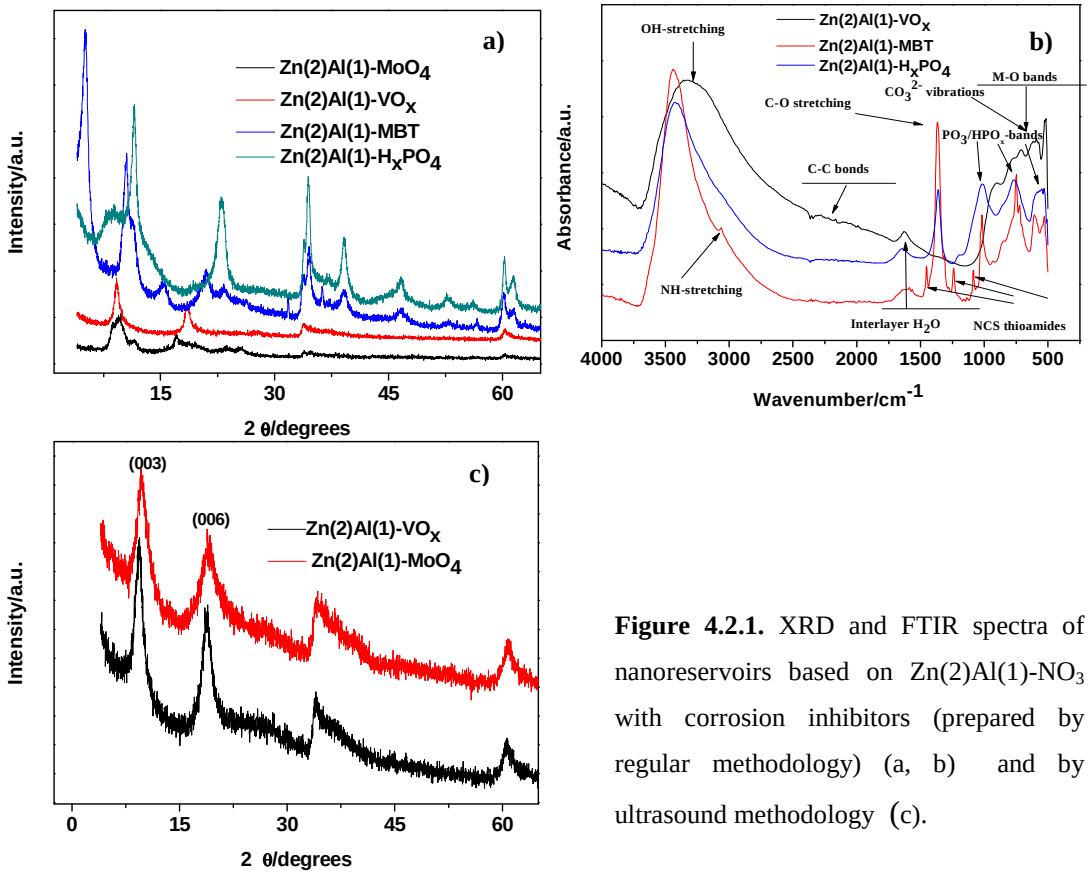

Figure 4.2.1. XRD and FTIR spectra of nanoreservoirs based on Zn(2)Al(1)-NO_3 with corrosion inhibitors (prepared by regular methodology) (a, b) and by ultrasound methodology (c).

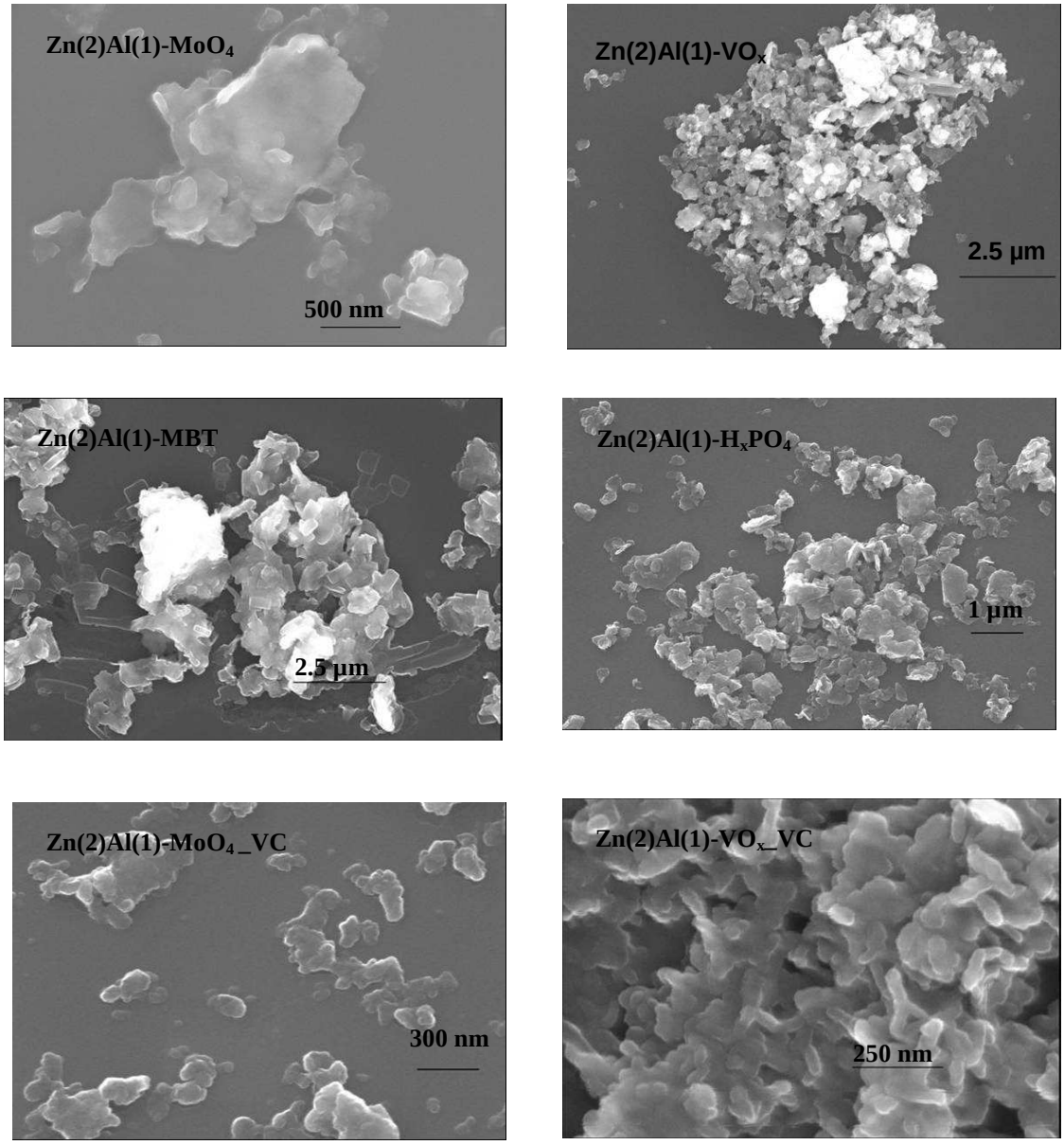

Figure 4.2.2. Morphological characterization of nanoreservoirs by SEM.

Table 4.2.1. Representative parameters calculated from XRD data of LDHs intercalated with corrosion inhibitors.

Composition	Average crystallite size, nm	Basal spacing, nm
Zn(2)Al(1)-MoO_4	-	0.94
Zn(2)Al(1)-VO_x	8.10	0.94
Zn(2)Al(1)-MBT	-	1.72
Zn(2)Al(1)-H_xPO_4	7.40	1.06
Zn(2)Al(1)-MoO_4 (ultrasound)	4.50	0.91
Zn(2)Al(1)-VO_x (ultrasound)	5.80	0.97

Analysis of the XRD results reveals the displacement of the diffraction peaks positions of LDHs intercalated with corrosion inhibitors to lower 2θ values. This suggests an increase of basal spacings (Table 4.2.1.). The absence of reflections associated with Zn(2)Al(1)-NO_3 LDH indicates that ion exchange reaction has been completed.

The pH of anion exchange reaction with molybdate anions is 9.2. The XRD pattern of Zn(2)Al(1)-MoO_4 (regular synthesis) demonstrate additional peaks which can be attributed to other LDH phase. Overlapped broad peaks made impossible estimation of average size of crystallites in this sample (not indicated in Table 4.2.1). In the case of LDHs intercalated with vanadates VO_x is used in the formula of the prepared LDHs instead of VO_3^-. This is related to pH-dependent speciation of VO_x [95]. In this work the pH of ion-exchange reaction for vanadates was 8.4. At this pH the predominant vanadate species are $V_2O_7^{4-}$ and $HV_2O_7^{3-}$. The dimensions of $V_2O_7^{4-}$ anion corresponding to perpendicular and parallel arrangements in interlayer are 0.78 and 0.50 nm, respectively. In the present work, the gallery height determined for LDH-VO_x was found to be 0.46 nm, meaning that the most likely configuration of these anions is the parallel arrangement with respect to LDH layers. Since the anion $HV_2O_7^{3-}$ is formed by protonating one of the terminal oxygens in $V_2O_7^{4-}$, the gallery height is not expected to change much. Hence VO_x can be associated with one of these possible vanadate polytypes. The results of ICP measurements have also confirmed a Zn:Al ratio in the Zn(2)Al(1)-VO_x LDH as 2:1, meaning that during the ion-exchange reaction the hydroxide layers were enough stable.

The presence of (at least) two anionic forms is also possible for phosphates. Ion-exchange reaction in this case was performed at pH 7, at which HPO_4^{2-} and $H_2PO_4^-$ co-exist. This is the reason for phosphate anions in the LDH structure being labelled as H_xPO_4. Badreddine and others [36] investigated the intercalation of phosphates (with different charges and sizes) into the structure of Zn(2)Al(1)-Cl LDHs. The value of basal spacing obtained in the present work (1.06 nm) is in agreement with the values reported by Badreddine (1.06 nm for HPO_4^{2-}). The presence of these anions in LDHs is also confirmed from the FTIR spectra.

In the case of LDH-MBT synthesis the pH of ion-exchange was chosen to be 10, to guarantee that the predominating species are mercaptobenthiazolate anions and also to increase the solubility of MBT in solution. The value of basal spacing for this type of LDH is higher than for Zn(2)Al(1)-VO_x and Zn(2)Al(1)-H_xPO_4 (1.72 nm), which is expected from the difference in relative sizes of the intercalating anions [74]. For all the LDHs nanocontainers there is a decrease of average crystallite size when ion-exchange occurs. It has been recently shown [96] that anion exchange nitrate –vanadate in Zn–Al LDHs leads to irreversible decrease of the average size of crystallites as a result of mechanical fragmentation of the crystallites. The fragmentation occurs due to fast anion exchange in the initial stage of the process. Since nitrate anion is easy exchangeable, such a fragmentation can be expected in other exchange processes where Zn(2)Al(1)-NO_3 is a parent composition.

The values of basal spacings for LDHs prepared under ultrasound conditions are in agreement with the values for for the respective compositions prepared using the regular methodology. The average crystallite size is lower for Zn(2)Al(1)-VO_x synthesized in the vibrating cell is smaller in comparison to those obtained by regular synthesis, which is in agreement with that observed in the precursor samples prepared by using these two methodologies. For Zn(2)Al(1)-MoO_4 LDHs prepared under ultrasound conditions a single-phased material with the average crystallite size value 4.2 nm was obtained.

Analysis of the FTIR spectra of nanoreservoirs provides additional structural characterization of the samples. The obtained results are in agreement with literature data [32, 36, 97, 98-100]. The following bands are presented in all structures: 3600-3300 cm^{-1} - OH vibrations; 1640-1620 cm^{-1} - interlayer water molecules; 1335, 874 and 671 cm^{-1} - CO

stretching (indication of partial presence of carbonates between LDHs layers, probably caused during storage conditions); below 800 cm^{-1} - vibration of metal-oxygen bonds. Intercalation of guest species is indicated by vibrations of specific groups. The band at 3113 cm^{-1} is associated with NH-stretching; 1321-1247 cm^{-1} and 1078-1014 cm^{-1} are attributed to NCS thioamides I, II, III respectively and confirm the presence of MBT in the interlayer gallery. Broadening of the OH-band for Zn(2)Al(1)-H_xPO_4 is possibly caused by the formation of hydrogen bonds between the phosphate groups and water molecules in the LDHs layers [36]. The vibrations of assigned to phosphates confirm their presence in the LDH structure.

SEM images reveal that after ion-exchange the LDHs still show a plate-like morphology. However, the particle size distribution determined by DLS depends on the type of intercalated anions (Table 4.2.2. and Figure 4.2.3.). This may be related to the fact that the intercalating anions will change the Zeta-potential as shown in Table 4.2.2. and in some cases agglomeration of LDH particles will occur. The range of agglomerates diameter varies from submicron to 1.5 - 2 μm. For Zn(2)Al(1)-VO_x prepared under ultrasound conditions it is around 500 nm.

The values of zeta-potential reveal a decrease of stability of nanoreservoirs colloidal systems in H_2O, in comparison to LDH-NO_3 precursors. These results show that values of particle size diameters can be more accurately estimated from the SEM measurements, because instability of these LDHs in water complicates the correct assessment of this parameter.

Table 4.2.2. Colloidal properties of LDHs nanoreservoirs.

Composition	**Maxima of particle size distribution, nm**	**Zeta potential, mV**
Zn(2)Al(1)-MoO_4	459.00 ; 1480.00 *	+27.30
Zn(2)Al(1)-VO_x	1990.00*	+1.72
Zn(2)Al(1)-MBT	1480.00*	+29.00
Zn(2)Al(1)-H_xPO_4	1280.00;5560.00	-17.40
Zn(2)Al(1)-MoO_4 (ultrasound)	4800.00*	+12.50
Zn(2)Al(1)-VO_x (ultrasound)	459.00	-13.60

***** estimation is complicated, because of colloidal instability of the system

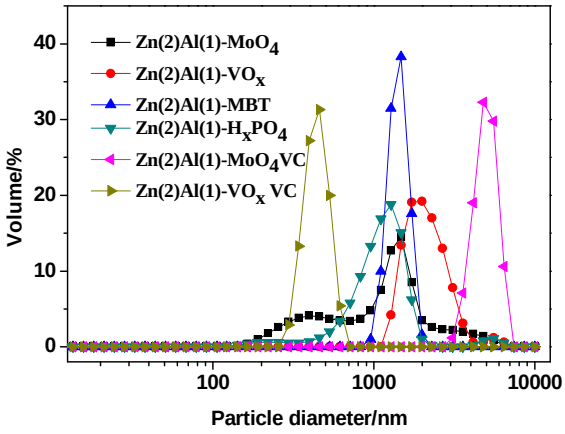

Figure 4.2.3. Particle size distribution of nanoreservoirs based on Zn(2)Al(1)-NO_3 precursor with corrosion inhibitors.

Figure 4.2.4. presents the structure, morphology and particle size distribution of nanoreservoirs loaded with corrosion inhibitors, prepared from Mg(2,3)Al(1)-NO_3 and Zn(2)Cr(1)-NO_3 precursors. Table 4.2.3. shows some parameters of the LDH nanoreservoirs obtained from XRD data and DLS measurements. The ion-exchange reactions of Mg-Al-NO_3 and Zn-Cr-MoO_4 LDHs with MBT^- and MoO_4^{2-} were held at the same conditions like those mentioned for Zn(2)Al(1)-NO_3 precursor, namely at pH = 10 and pH = 9.2, respectively.

The XRD patterns and the basal spacings of the nanoreservoirs are in agreement with the ones obtained for LDHs based on Zn(2)Al(1)-NO_3 precursor intercalated with MBT anions. Positions of diffraction peaks shift to lower 2θ values upon exchange. In the XRD patterns of Mg(2,3)Al(1)-MBT additional peaks (similar to those observed in Zn(2)Al(1)-MBT) indicate that these samples contain two LDH phases. The values of average crystallite size (presented in Table 4.2.3.) were calculated for the main phase. The appropriate vibration bands of MBT are indicated in the FTIR pattern (together with small carbonate vibrations and bonds of interlayer water).

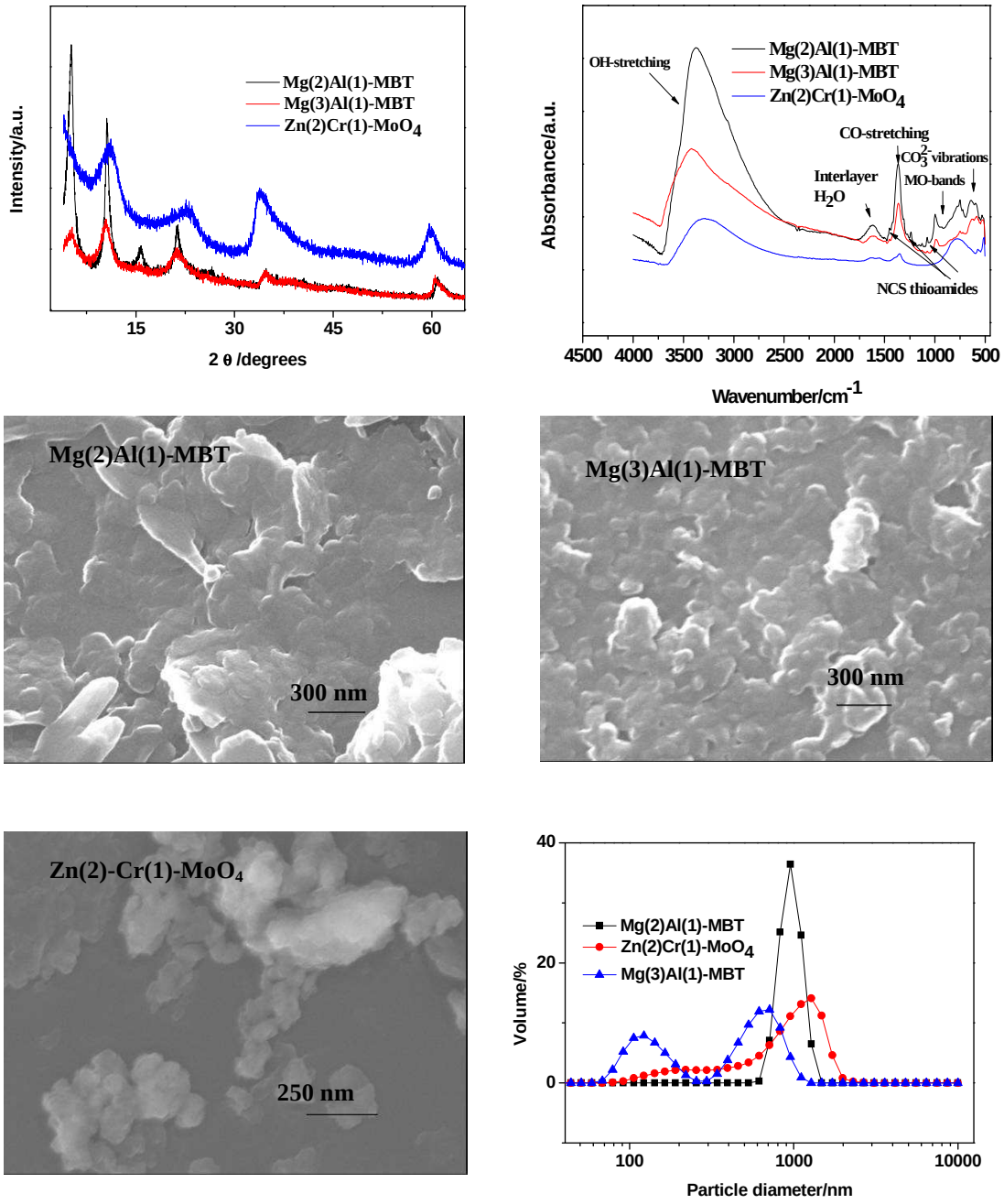

Figure 4.2.4. XRD, FTIR patterns, SEM images and particle size distribution of nanoreservoirs with corrosion inhibitors based on Mg(x)Al(1)-NO_3; x =2,3 and Zn(2)Cr(1)-NO_3 precursors.

Table 4.2.3. Parameters of LDH nanoreservoirs evaluated from XRD and DLS measurements.

Compound	Average crystallite size, nm	Basal spacing, nm	Maxima of particle size distribution, nm	Zeta potential, mV
Mg(2)Al(1)-MBT	8.60	1.70	955.00*	+26.50
Mg(3)Al(1)-MBT	4.20	1.69	122.00; 712.00	+39.60
Zn(2)Cr(1)-MoO_4	2.30	0.82	396.00;1280.00	+34.10

* estimation is complicated, because of colloidal instability of the system

Zn(2)Cr(1)-MoO_4 was obtained as a single-phase LDH with the average crystallite size value of 2.3 nm and slightly lower basal spacing in comparison with Zn(2)Al(1)-MoO_4 nanoreservoir. Its FTIR spectra contain very small vibrations associated with CO bonds.

In the nanoresevoirs Mg(2)Al(1)-MBT, Zn(2)Cr(1)-MoO_4 and Mg(3)Al(1)-MBT, like in the respective LDHs based on the Zn(2)Al(1)-NO_3 precursor, a decrease in average crystallite size as a result of anion exchange was observed.

Analysis of Zeta-potential values shows that Mg/Al-MBT nanoreservoirs are unstable in water and the values of particle diameter can be only properly estimated using SEM images. On the contrary, Zn(2)Cr(1)-MoO_4 system is stable in water (Zeta potential is above +30 mV). Similar to nanocontainers based on Zn(2)Al(1)-NO_3 precursor, Mg-Al and Zn-Cr LDHs preserve plate-like morphology upon ion-exchange.

Part II. Preparation of nanoreservoirs by calcination-rehydration methodology

4.3 Preparation of LDH precursor

Commercial synthetic hydrotalcite (referred hereafter as SH with formula - $[Mg_6Al_2(OH)_{16}CO_3 \cdot 4H_2O]$) in powder form was used as precursor in the calcination – rehydration methodology (procedure conditions are described in the Experimental part). Figure 4.3.1. shows the XRD pattern and morphology of SH, as well as its particle size distribution.

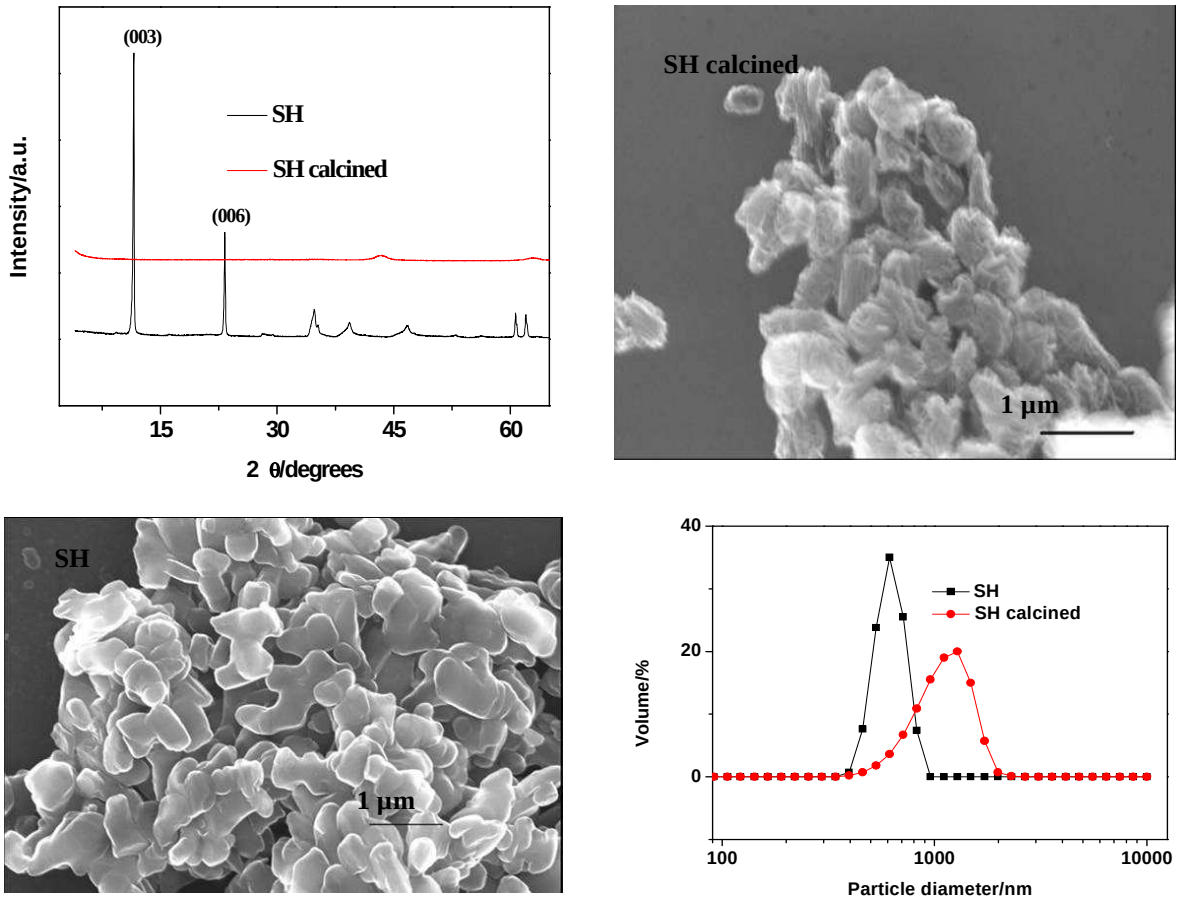

Figure 4.3.1. XRD pattern, SEM images and graph of particle size distribution of SH calcined.

It is seen from XRD data that calcination of SH results in decomposition of LDH structure. The SEM image also reveals the absence of typical plate-like morphology for LDHs. After calcination it changes to spheroid particles with the diameter typically around 500 nm. The value of Zeta-potential of water suspension of calcined SH is +40.1 mV and maximum of particle size distribution detected by DLS is around 1.3 μm. For SH the maximum of particle size distribution is about 615 nm and value of Zeta potential is +7.13 mV. The low value of zeta potential shows that SH is not stable in H_2O, which is in agreement with visual inspection of the sample (SH could not be completely dispersed in H_2O). Therefore, the obtained particle size distribution is not representative of SH system.

4.4.Preparation of nanoreservoirs with corrosion inhibitors

The reconstruction of LDH structure from calcined SH was performed by using solutions of the following corrosion inhibitors: MoO_4^{2-} (Na_2MoO_4), VO_3^- ($NaVO_3$), MBT^- (2-mercaptobenzothiazole) and HPO_4^{2-} (Na_2HPO_4). Characterization of these nanoreservoirs is presented in Figure 4.4.1.

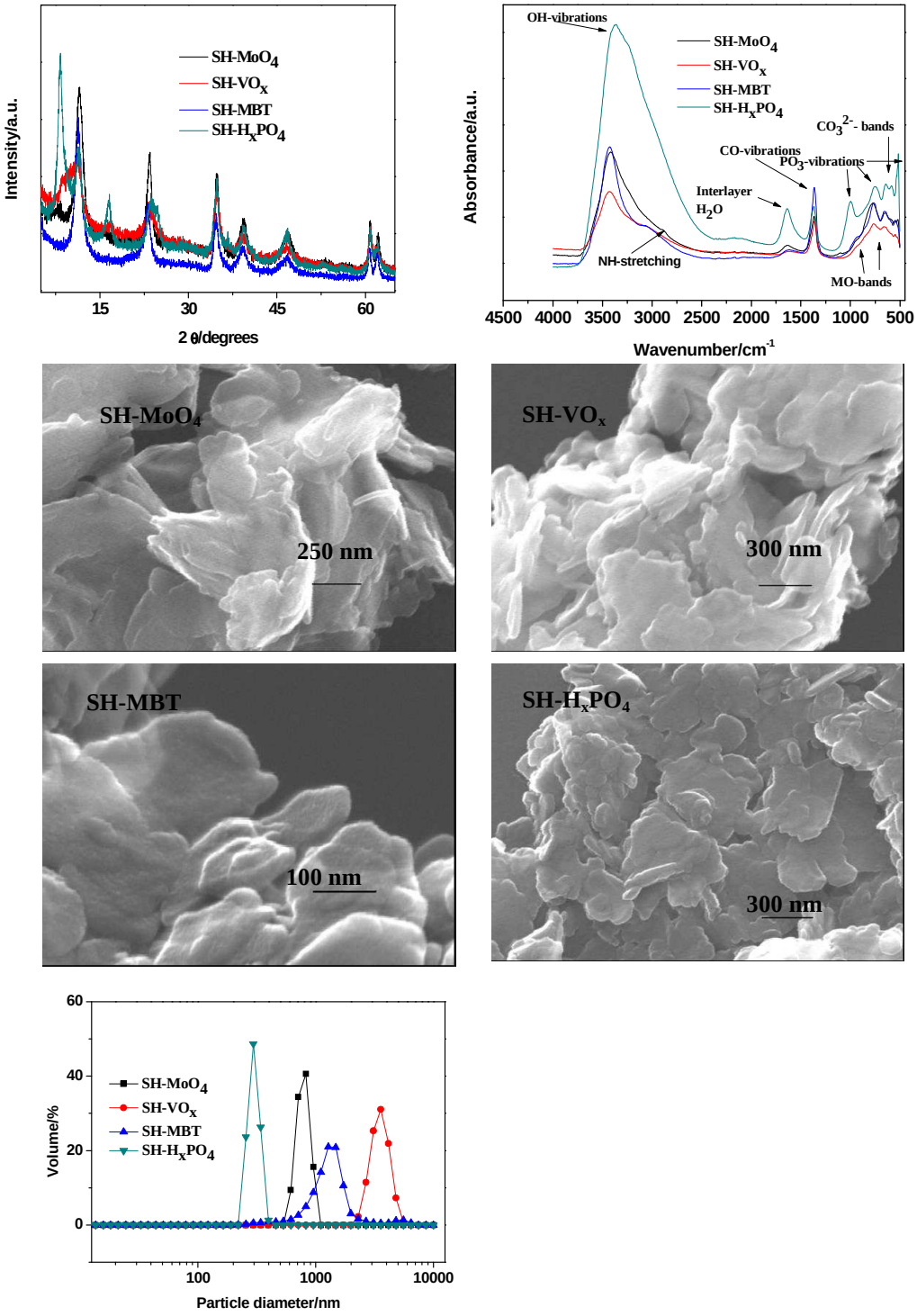

Figure 4.4.1. XRD patterns, FTIR spectra, SEM images with particle size distribution of LDH nanoreservoirs prepared by calcination-rehydration methodology.

Some parameters obtained from XRD data and DLS are collected in Table 4.4.1.

Table 4.4.1. Parameters of LDH nanoreservoirs prepared by calcination-rehydration methodology evaluated from XRD and DLS measurements.

Compound	Average crystallite size, nm	Basal spacing, nm	Maxima of particle size distribution, nm	Zeta potential, mV
SH-MoO_4	11.00	0.77	825.00*	+14.10
SH-VO_x	10.40	0.77	3580.00	- 9.02
SH-MBT	8.70	0.78	1280.00; 5560.00	+42.10
SH-H_xPO_4	10.60	1.06	295.00*	+5.14

***** estimation is complicated, because of colloidal instability of the system

XRD measurements reveal that rehydration results in reconstruction of LDH structure in all the LDH nanoreservoirs under study. However, the values of basal spacing for nanoreservoirs loaded with molybdates, vanadates and MBT anions are the same (within the experimental error). In fact, these values are close to the basal spacing value of initial synthetic hydrotalcite, Mg(3)Al(1)-CO_3 (0.76 nm [101, 102]). On the other hand, the observed values of basal spacing can be associated with intercalated OH^- anions (0.72-0.79 nm [26, 103]). Presence of OH^- in the interlayers is more likely, because the concentration of this anion in the environment at the rehydration is higher than that of carbonate. Therefore, intercalation of corrosion inhibitors *within* the interlayer galleries by this methodology was not successful for the majority of corrosion inhibitors, although adsorption of inhibitors on LDHs surface is expected as shown in FTIR spectra.

The basal spacing for the SH-H_xPO_4 is in agreement with the literature [36] and is identical to that like for Zn(2)Al(1)-H_xPO_4 LDH, showing that in this case intercalation was successful. This is also confirmed by vibrations assigned to phosphate species in the FTIR spectrum. Similar to Zn(2)Al(1)-H_xPO_4, the broadening of OH-vibration can indicate establishment of hydrogen bonds between water molecules and phosphates [36].

Furthermore, SEM images confirm reconstruction of LDH plate-like morphology. The diameters of agglomerates can be estimated in the following range: for SH-MoO_4 it is about 700 nm, for SH-VO_x and SH-H_xPO_4 about 500 nm and for SH-MBT ca. 200 nm. Values of Zeta potential for most of these nanoreservoirs (except for SH-MBT) confirm a high tendency to agglomeration of the LDH particles.

The rehydration step is a complex process. Different factors can influence the formation of LDH structure, including different affinities of competing anions and the relative concentration. The LDH structure has strong affinity for intercalation of OH^- and CO_3^{2-} anions in comparison to corrosion inhibitors [14, 26]. On the other hand, successful rehydration depends on the calcination temperature [17]. Therefore, the calcination-rehydration process needs to be further investigated and the experimental procedure optimized to achieve successful intercalation of corrosion inhibitors (e.g. composition of LDH precursor, temperature of calcination, pH, composition of aqueous solution used in the rehydration step). However, the main advantage of this methodology consists in the possibility of large scale production of LDHs.

Part III. Thermal characterization of LDHs

4.5. TG/DTA measurements

The thermal characterization of LDHs was performed for the representative system (Zn(2)Al(1)-NO_3) prepared by regular coprecipitation. According to literature data available [104, 105] the thermal degradation of LDHs occurs typically in four steps: (i) desorption of physically adsorbed water; (ii) removal of water from interlayer galleries; (iii) dehydroxylation of brucite-like layers; (iv) decomposition of interlayer anions. Heating up to 250 ^{0}C leads to release of interlayer water, further increase of temperature up to 450^{0}C causes dehydroxylation of hydroxide layers and decomposition of interlayer anion of the interlayer space. The thermal stability of different LDHs increases in the following order [26]:

Co–Al < Zn–Al ≈ Cu–Al < Mg–Fe ≈ Ni–Al < Mg–Al ≈Mg–Cr

Thermal decomposition of LDHs is dependent upon the type of presented cations in the hydroxides layers as well as on the structure and arrangement of interlayer anion.

For Zn/Al LDHs, the removal of superficially adsorbed water is expected to occur in the range 25-70 ºC [106], further heating from 100^{0}C to 180^{0}C removes physically adsorbed water and intergallery water. The endothermic peaks in DTA spectrum in the temperature range between 180-290 ^{0}C are assigned to dehydroxylation of OH^- lattice, and between 290-550 ^{0}C to decomposition of interlayer anion [67, 104]. The arrangement of the interlayer nitrates influences the thermal behavior of NO_3^- incorporated into LDHs. The distribution of nitrates in the interlayer space can change from “flat-lying” to “stick-lying” with the increase of nitrate anions within the galleries. The dehydroxylation process is retarded when nitrates are arranged in the stick-lying conformation, alternately attaching to top and bottom hydroxyl sheets of contiguous layers [26, 107].

Figure 4.5.1. shows TG/DTA spectra for Zn(2)Al(1)-NO_3. In the beginning, the sample weight was 33.4 mg. In the DTA spectrum several endothermic peaks can be observed in the temperature range from 50 ^{0}C to 265 ^{0}C, namely at 95 ^{0}C, 170 ^{0}C, 235 ^{0}C and 263^{0}C, further heating will lead to decomposition of nitrate anions. This is in agreement with literature data [26, 67, 104, 106-109].

Analysis of the TG spectra shows that in the interval of temperatures up to 170^{0}C mass loss is about 8 %. This attributed to loss of superficially and physically adsorbed

water and interlayer water. The second mass loss during heating up to 263^{0}C (dehydroxylation of the hydroxide layers) corresponds to about 19 %. The splitting of peaks in the DTA spectrum at 235 and 263 ^{0}C can be associated to hydroxylation process of divalent and trivalent cations in the LDH structure [26]. The last mass loss (5.5 %) corresponds to decomposition of nitrates.

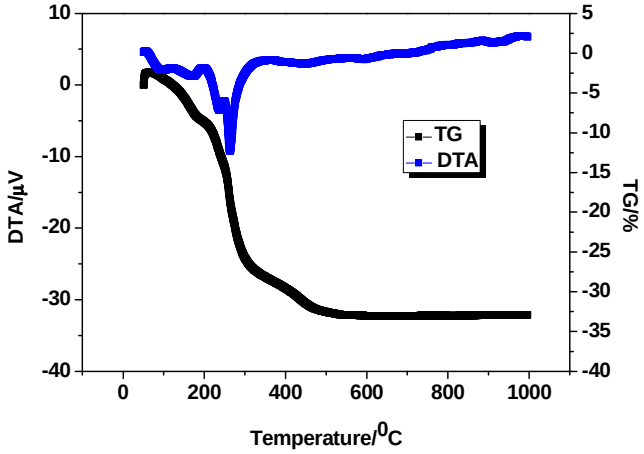

Figure 4.5.1. TG/DTA analysis of Zn(2)Al(1)-NO_3 LDH

Taking into account the initial mass of LDH for TG/DTA analysis (33.4 mg) and values of mass losses in every step it is possible to calculate the amount of substance corresponding to the total amount of water and amount of substance of nitrates in the LDH structure: n (H_2O) = 0.148 mmol; n(NO_3^-) = 0.029 mmol.

Conclusions

Several types of LDH materials intercalated with corrosion-inhibitors were successfully synthesized. These nanoreservoirs were prepared by two methodologies (coprecipitation/ion-exchange and calcination-rehydration), based on four LDH precursors with four different intercalating inhibitors. Particular attention was given to influence of various conditions on the precursor preparation, due to necessity of appropriate particle size distribution and colloidal properties of the final nanocontainers for their subsequent application in the anticorrosion coatings. The most important parameter for decreasing particle size has been found to be the application of ultrasound during the coprecipitation step.

Structure, morphology and colloidal properties of synthesized nanoreservoirs were characterized by several techniques including X-ray diffraction, Fourier transform infrared spectroscopy, SEM, dynamic light scattering. The prepared nanoreservoirs have a plate like morphology and the zeta potential depends on the type of cations that form LDH sheets and type of anions in the interlayer gallery. Additionally, the structural formula of Zn(2)Al(1)-NO_3 LDH precursor was estimated by ICP spectroscopy and TG/DTA measurements. The obtained TG/DTA results are in good agreement with literature data.

The success of inhibitor intercalation on LDHs was found to be dependent on the synthesis route. In the case of synthesis by coprecipitation/ion exchange, all the used inhibitors were intercalated whereas in the case of calcination-rehydration of synthetic hydrotalcite, only H_xPO_4 was successfully intercalated.

FUTURE GUIDELINES:

Further investigations of nanoreservoirs with corrosion inhibitors based on LDHs will be continued in the frame of my PhD thesis and will be devoted to synthesis of LDH nanoreservoirs by different methodologies with various inorganic and organic anionic corrosion inhibitors using the same LDH parent structure (Mg-Al and Zn-Al hydroxide layers) and preparation of LDHs with other cationic structures. Special attention will be paid on the release studies of the active species (corrosion inhibitors) in different conditions relevant for the occurrence of corrosion activity in metallic substrates. Other investigations will include surface modification of LDHs for tuning of the release triggering conditions for improvement of LDHs stabilization in coating formulations and

determination of anticorrosion efficiency of LDH-loaded inhibitors with respect to different metallic substrates.

References

1. E. McCafferty, “Introduction to corrosion science”, Springer Science+Business Media LLC, (2010) 575
2. P.R. Roberge, “Corrosion engineering. Principles and practice”, The McGraw-Hill Companies Inc., (2008) 754
3. A. Groysman, “Corrosion for everybody”, Springer Science+Business Media B.V., (2010) 368
4. M. L. Zheludkevich, “Self-healing anticorrosion coatings”, Self-healing materials S. K. Ghosh (Ed.) Wiley-VCH (2008) 101-139
5. M. L. Zheludkevich, I. M. Salvado and M. G. S. Ferreira, “Sol–gel coatings for corrosion protection of metals”, Journal of Materials Chemistry, 15 (2005) 5099–5111
6. Z. Li and C. Wang, “Si-W-P corrosion inhibitor used in desalted circulating cooling water system”, CN patent 101353204 (2009)
7. H. Cao, “Customized production and complete set of application technology of high performance low-phosphorous water treatment agent for treating circulating cooling water”, CN patent 101428910 (2009)
8. S. R. Tayler and B. D. Chambers, “Synergistic combinations of chromate free corrosion inhibitors”, US patent 0000958 (2009)
9. A. Aballe, M. Bethencourt, F.J. Botana and M. Marcos, “$CeCl_3$ and $LaCl_3$ – binary solutions as environment-friedly corrosion inhibitors of AA5083 Al-Mg alloy in NaCl solutions”, Journal of Alloys and Compounds 323–324 (2001) 855–858
10. D. G. Shchukin, M. Zheludkevich, K. Yasakau, S. Lamaka, M. G. S. Ferreira and H. Möhwald, “Layer-by-Layer Assembled Nanocontainers for Self-Healing Corrosion Protection”, Advanced Materials 18 (2006) 1672-1678
11. M. L. Zheludkevich, D. G. Shchukin, K. A. Yasakau, H. Möhwald and M. G. S. Ferreira, “Anticorrosion Coatings with Self-Healing Effect Based on Nanocontainers Impregnated with Corrosion Inhibitor”, Chemistry of Materials 19 (2007) 402-411
12. Y. Gao, X. Chen, B. Liao, X. Ding, Z. Zheng, X. Cheng, H. Pang and Y. Peng, “Polyelectrolyte Self-assembly Approach to Smart Nanocontainers”, Polymer Bulletin, 56 (2006) 305–311

13. C. Giacomelli, V. Schmidt and Redouane Borsali, “Nanocontainers Formed by Self-Assembly of Poly(ethyleneoxide)-b-poly(glycerol monomethacrylate)-Drug Conjugates”, Macromolecules, 40 (2007) 2148-2157
14. S. P. Newman and W. Jones, “Synthesis, characterization and applications of layered double hydroxides containing organic guests”, New Journal of Chemistry (1998) 105-115
15. G. R. Williams and D. O’Hare, “Towards understanding, control and application of layered double hydroxide chemistry”, Journal of Materials Chemistry 16 (2006) 3065-3074
16. D. G. Evans and R. C. T. Slade, “Structural Aspects of Layered Double Hydroxides”, Structure and Bonding 119 (2006) 1-87
17. J. He, M. Wei, B. Li, Y. Kang, D. G. Evans and X. Duan, “Preparation of Layered Double Hydroxides”, Structure and Bonding 119 (2006) 89-119
18. F. Leroux and J.-P. Besse, “Polymer Interleaved Layered Double Hydroxide: A New Emerging Class of Nanocomposites”, Chemistry of Materials, 13 (2001) 3507-3515
19. P. Porta and S. Morpurgo, “Cu/Zn/Co/Al/Cr-containing hydrotalcite-type anionic clays”, Applied Clay Science 10 (1995) 31-44
20. J. Das, D. Das and K.M. Parida, “Preparation and characterization of Mg–Al hydrotalcite-like compounds containing cerium”, Journal of Colloid and Interface Science 301 (2006) 569–574
21. Z. Chang, D. Evans, X. Duan, P. Boutinaud, M. de Roy and C. Forano, “Preparation and characterization of rare earth-containing layered double hydroxides”, Journal of Physics and Chemistry of Solids 67 (2006) 1054–1057
22. S. Velu, D. P. Sabde, Neepa Shah, and S. Sivasanker, “New Hydrotalcite-like Anionic Clays Containing Zr^{4+} in the Layers: Synthesis and Physicochemical Properties”, Chemistry of Materials, 10 (1998) 3451-3458
23. S.-Y. Kwak, Y.-J. Jeong, J.-S. Park and J.-H. Choy, “Bio-LDH nanohybrid for gene therapy”, Solid State Ionics 151 (2002) 229– 234
24. S. K. Yun and T. J. Pinnavaia, “Layered Double Hydroxides Intercalated by Polyoxometalate Anions with Keggin(r-$H_2W_{12}O_{40}^{6-}$), Dawson (r-$P_2W_{18}O_{62}^{6-}$), and

Finke ($Co_4(H_2O)_2(PW_9O_{34})_2^{10-}$) Structures, Inorganic Chemistry, 35 (1996) 6853-6860

25. A.I. Khan and D.O'Hare, "Intercalation Chemistry of Layered Double Hydroxides: Recent Developments and Applications", Journal of Materials Chemistry, 12 11 (2002) 3191-3198
26. F. Bergaya, B.K.G. Theng and G. Lagaly, "Handbook of clay science", Elsevier Ltd (2006) 1125
27. I. Pausch, H. H. Lohse, H.H., K. Schürmann and R. Allmann,. "Syntheses of disordered and A1-rich hydrotalcite-like compounds", Clays and Clay Minerals 34, (1986) 507–510
28. O. Clause, B. Rebours, E. Merlen, F. Trifiró and A. Vaccari, "Preparation and characterization of nickel–aluminum mixed oxides obtained by thermal decomposition of hydrotalcite-type precursors". Journal of Catalysis 133 (1992) 231–246
29. I. Crespo, C. Barriga, V Rives and M.A. Ulibarri, "Intercalation of iron hexacyano complexes in Zn,Al-hydrotalcite", Solid State Ionics 101-103 (1997) 729-735
30. P. Benito, I. Guinea, M. Herrero, F. M. Labajos, and V. Rives, "Incidence of Microwave Hydrothermal Treatments on the Crystallinity Properties of Hydrotalcite-like Compounds", Journal of Inorganic and General Chemistry. (2007) 1815-1819
31. P. Benito, F. M. Labajos, and V. Rives, "Microwaves and layered double hydroxides: A smooth understanding", Pure and Applied. Chemistry., 81 8 (2009) 1459–1471
32. D.-Y. Wang, F. Reny Costa, A. Vyalikh, A. Leuteritz, U. Scheler, D. Jehnichen, U. Wagenknecht, L. Haussler and G. Heinrich, "One-Step Synthesis of Organic LDH and Its Comparison with Regeneration and Anion Exchange Method", Chemistry of Materials, 21 (2009) 4490–4497
33. M. Meyn, K. Beneke and G. Lagaly, "Anion-Exchange Reactions of Layered Double Hydroxides", Inorganic Chemistry, 29 (1990), 5201-5207
34. G. Arizaga, A. Mangrich, J. Gardolinski and F. Wypych, "Chemical modification of zinc hydroxide nitrate and Zn–Al-layered double hydroxide with dicarboxylic acids", Journal of Colloid and Interface Science 320 (2008) 168–176

35. F. Wypych, G. Arízaga and J.Gardolinski “Intercalation and functionalization of zinc hydroxide nitrate with mono and dicarboxylic acids”, Journal of Colloid and Interface Science 283 (2005) 130–138
36. M. Badreddine, A. Legrouri, A. Barroug, A. De Roy and J.P. Besse, “Ion exchange of different phosphate ions into the zinc–aluminium–chloride layered double hydroxide”, Materials Letters 38 (1999) 391-395
37. S. Carlino, M. J. Hudson, S. W. Husain and J. A. Knowles, “The reaction of molten phenylphosphonic acid with a layered double hydroxide and its calcined oxide”, Solid State lonics 84 (I 996) 117- 129
38. T. S. Stanimirova, I. Vergilov, G. Kirov and N. Petrova, “Thermal decomposition products of hydrotalcite-like compounds: low-temperature metaphases”, Journal of Materials Science 34 (1999) 4153–4161
39. O. Clause, M. Gazzano, F. Trifiró, A. Vaccari and L. Zatorski, “Preparation and thermal reactivity of nickel/chromium and nickel/aluminium hydrotalcite-type precursors”. Applied Catalysis 73 (1991) 217–236
40. J. T. Kloprogge and R. L. Frost, “Infrared and Raman spectroscopic studies of layered double hydroxides (LDHs)”, Layered Double Hydroxides, V. Rives Nova Science Publishers, Huntington (2001) 139–192
41. J. T. Kloprogge, L. Hickey and R. L. Frost, “Heating stage Raman and infrared emission spectroscopic study of the dehydroxylation of synthetic Mg-hydrotalcite”, Applied Clay Science 18 (2001) 37–49
42. T. S. Stanimirova, G. Kirov and E. Dinolova, “Mechanism of hydrotalcite regeneration”, Journal of Materials Science Letters 20 (2001) 453–455
43. S. Carlino and M. J. Hudson, “Reaction of Molten Sebacic Acid with a Layered (Mg/AI) Double Hydroxide”, Journal of Materials Chemistry, 4 1 (1994) 99-104
44. S. Carlino and M. J. Hudson, “Thermal Intercalation of Layered Double Hydroxides: Capric Acid into an Mg-AI LDH”, Journal of Materials Chemistry, 5 9 (1995) 1433-1442
45. A. Inayat, M. Klumpp and W. Schwieger, “The urea method for the direct synthesis of ZnAl layered double hydroxides with nitrate as the interlayer anion”, Applied Clay Science 51 (2011) 452–459

46. T. Hibino and H. Ohya, “Synthesis of crystalline layered double hydroxides: Precipitation by using urea hydrolysis and subsequent hydrothermal reactions in aqueous solutions”, Applied Clay Science 45 (2009) 123–132
47. Y. Arai and M. Ogawa, “Preparation of Co–Al layered double hydroxides by the hydrothermal urea method for controlled particle size”, Applied Clay Science 42 (2009) 601–604
48. G. V. Manohara and P. V. Kamath, “Synthesis and structure refinement of layered double hydroxides of Co, Mg and Ni with Ga”, Bulletin of. Material. Science., 33 3, (2010). 325–331
49. Y. Zhao, F. Li, R. Zhang, D. G. Evans, and X. Duan, “Preparation of Layered Double-Hydroxide Nanomaterials with a Uniform Crystallite Size Using a New Method Involving Separate Nucleation and Aging Steps”, Chemistry of. Materials; 14 (2002) 4286-4291
50. K. Cho, Y. Lin, D. G. Evans and D. Li, “Preparation and photochromic properties of NiAl-NO3-LDHs/LDPE composite”, Chinise Science Bulletin, 52 7 (2007) 877-882
51. G. Hu, N. Wang, D. O’Hare and J. Davis, “Synthesis of magnesium aluminium layered double hydroxides in reverse microemulsions”, Journal of Materials Chemistry, 17 (2007) 2257–2266
52. G. Hu and D. O’Hare, “Unique Layered Double Hydroxide Morphologies Using Reverse Microemulsion Synthesis”, Journal of American Chemical Society, 127 (2005) 17808-17813
53. J. He, B. Li, D. G. Evans and X. Duan, “Synthesis of layered double hydroxides in an emulsion solution”, Colloids and Surfaces A: Physicochemical and. Engineering. Aspects 251 (2004) 191–196
54. F. Li and X. Duan, “Applications of Layered Double Hydroxides”, Structure and Bonding 119 (2006) 193-223
55. A. Dubey, “Synthesis and catalytic applications of CMK-LDH (layered double hydroxides) nanocomposite materials”, Green Chemistry, 9 (2007) 424–426
56. Z. P. Xu, J. Zhang, M. O. Adebajo, H. Zhang and C. Zhou, “Catalytic applications of layered double hydroxides and derivatives”, Applied Clay Science 53 (2011) 139–150

57. A. Béresa, I. Pálinkó, I. Kiricsia, J. B. Nagy, Y. Kiyozumid and F. Mizukami, “Layered double hydroxides and their pillared derivatives-materials for solid base catalysis; synthesis and characterization”, Applied Catalysis A: General 182 (1999) 237-247
58. J. Wang, Z. Lei, H. Qin, L. Zhang and F. Li, “Structure and Catalytic Property of Li-Al Metal Oxides from Layered Double Hydroxide Precursors Prepared via a Facile Solution Route”, Industrial and Engineering Chemistry Research (ASC publications) 51 (2011) 7120-7128
59. J. L. Shumaker, C. Crofcheck, S. A. Tackett, E. Santillan-Jimenez, T. Morgan, Y. Ji, M. Crocker and T. J. Toops “Biodiesel synthesis using calcined layered double hydroxide catalysts”, Applied Catalysis B: Environmental 82 (2008) 120–130
60. Y. Wang, W. Yang, C. Chen and D. G. Evans, “Fabrication and electrochemical characterization of cobalt-based layered double hydroxide nanosheet thin-film electrodes”, Journal of Power Sources 184 (2008) 682–690
61. H. Yin, L. Cui, S. Ai, H. Fan and L. Zhu, “Electrochemical determination of bisphenol A at Mg–Al–CO_3 layered double hydroxide modified glassy carbon electrode”, Electrochimica Acta 55 (2010) 603–610
62. Z.-A. Hu, Y.-L. Xie, Y.-X. Wang, H.-Y. Wu, Y.-Y. Yang and Z.-Y. Zhang, “Synthesis and electrochemical characterization of mesoporous Co_xNi_{1-x} layered double hydroxides as electrode materials for supercapacitors”, Electrochimica Acta 54 (2009) 2737–2741
63. F. Bruna, I. Pavlovic, C. Barriga, J. Cornejo and M.A. Ulibarri; “Adsorption of pesticides Carbetamide and Metamitron on organohydrotalcite”, Applied Clay Science 33 (2006) 116–124
64. I. Pavlovic, C. Barriga, M.C. Hermosín, J. Cornejo and M.A. Ulibarri, “Adsorption of acidic pesticides 2,4-D, Clopyralid and Picloram on calcined hydrotalcite”, Applied Clay Science 30 (2005) 125– 133
65. D. Chaara, I. Pavlovic, F. Bruna, M.A. Ulibarri, K. Draoui and C. Barriga; “Removal of nitrophenol pesticides from aqueous solutions by layered double hydroxides and their calcined products”, Applied Clay Science 50 (2010) 292–298
66. F. Bruna, R. Celis, I. Pavlovic, C. Barriga, J. Cornejo and M.A. Ulibarri, “Layered double hydroxides as adsorbents and carriers of the herbicide (4-chloro-2-

methylphenoxy)acetic acid (MCPA): Systems Mg–Al, Mg–Fe and Mg–Al–Fe", Journal of Hazardous Materials 168 (2009) 1476–1481

67. M. Islam and R. Patel, "Synthesis and physicochemical characterization of Zn/Al chloride layered double hydroxide and evaluation of its nitrate removal efficiency", Desalination 256 (2010) 120–128
68. Y. Seida and Y. Nakano, "Removal of phosphate by layered double hydroxides containing iron", Water Research 36 (2002) 1306–1312
69. J. Das, B. S. Patra, N. Baliarsingh and K. M. Parida, "Adsorption of phosphate by layered double hydroxides in aqueous solutions", Applied Clay Science 32 (2006) 252–260
70. C. Del Hoyo, "Layered double hydroxides and human health: An overview", Applied Clay Science 36 (2007) 103–121
71. S. Shafiei1, Z. T. Birgani, A. Darvish, M. S. Azimi and M. Solati-Hashjin, "Layered Double Hydroxides for Diagnostic Applications", International Congress of Evaluation of Medical Diagnosis Modern Technologies, (2008) 1-16
72. J.-H. Choy, J.-S. Jung, J.-M. Oh, M. Park, J. Jeong, Y.-K. Kang and O.-J. Han, "Layered double hydroxide as an efficient drug reservoir for folate derivatives", Biomaterials 25 (2004) 3059–3064
73. S. K. Poznyak, J. Tedim, L. M. Rodrigues, A. N. Salak, M. L. Zheludkevich, L. F. P. Dick and M. G. S. Ferreira, "Novel Inorganic Host Layered Double Hydroxides Intercalated with Guest Organic Inhibitors for Anticorrosion Applications", ACS Applied Materials and Interfaces 1 10 (2009) 2353-2362
74. J. Tedim, S. K. Poznyak, A. Kuznetsova, D. Raps, T. Hack, M. L. Zheludkevich and M. G. S. Ferreira, "Enhancement of Active Corrosion Protection via Combination of Inhibitor-Loaded Nanocontainers", ACS Applied materials and interfaces 2 5 (2010) 1528-1535
75. S. P. V. Mahajanam and R. G. Buchheit, "Characterization of Inhibitor Release from Zn-Al-$[V_{10}O_{28}]^{6-}$ Hydrotalcite Pigments and Corrosion Protection from Hydrotalcite- Pigmented Epoxy Coatings", Corrosion (2008) 230-240
76. M. A. Woo, T. Woo Kim, M.-J. Paek, H.-W. Ha, J.-H. Choy and S.-J. Hwang, "Phosphate-intercalated Ca–Fe-layered double hydroxides: Crystal structure,

bonding character and release kinetics of phosphate", Journal of Solid State Chemistry184 (2011) 171–176

77. Y. Leng, "Materials Characterization Introduction to Microscopic and Spectroscopic Methods", John Wiley & Sons (Asia) Pte Ltd (2008) 337
78. W. D. Callister Jr., "Materials Science and Engineering An Introduction", seventh edition, John Wiley & Sons, Inc (2007) 981
79. R. Guinebretière, "X-ray diffraction by polycrystalline materials", ISTE Ltd (2007) 351
80. V. K. Pecharsky and P. Y. Zavalij, "Fundamentals of powder diffraction and structural characterization of materials", Springer (2003) 713
81. N. B. Colthup, "Infrared Spectroscopy", Encyclopedia of Physical Science and Technology-Analytical Chemistry (2001) 793-816
82. R. B. King, "Encyclopedia of inorganic chemistry", Second edition,John Wiley (1994) 1-30
83. J. Goldstein, D. E. Newbury, P. Echlin, D. C. Joy, C. E. Lyman, E. Lifshin, L. Sawyer and J. R. Michael, "Scanning Electron Microscopy and X-Ray Microanalysis", third edition, Kluwer Academic/Plenum Publishers (2003) 689
84. R. Xu, "Particle characterization: dynamic light scattering methods", Kluwer Academic Publishers (2002) 391
85. B.J. Berne and R. Pecora, "Dynamic light scattering with applications to Chemistry, Biology and Physics", John Wiley Inc. (1976) 372
86. ZetaSizer Nano User Manual, Malvern Instruments Ltd. (2003, 2004, 2006, 2007, 2008) 10-54
87. C.-P. Sherman Hsu, "Infrared Spectroscopy", Handbook of instrumental techniques for Analytical Chemistry Prentice-Hall (1997) 247-283
88. www.ua.pt/lca/PageImages.aspx?id=6254
89. P. Gabbott, "Principles and applications of thermal analysis", Blackwell Publishing (2008) 464
90. M. E. Brown, "Introduction to thermal analysis. Techniques and applications", Kluwer Academic Publishers (2004) 264
91. Labsys, TG, DTA, DSC, TG-DTA and TG-DTS version Commissioning utilization 95

92. D. Myers, “Surfaces, Interfaces, and Colloids: Principles and Applications”, Second Edition, John Wiley & Sons, Inc (1999) 493
93. M. Elzbieciak, D. Wodka, S. Zapotoczny, P. Nowak and P. Warszynski, “Characteristics of Model Polyelectrolyte Multilayer Films Containing Laponite Clay Nanoparticles”, Langmuir American Chemical Society 26 1 (2010) 277–283
94. S. S. Batsanov, “Van der Waals Radii of Elements”, Inorganic Materials, 37 9 (2001). 871–885
95. M. Iannuzzi, T. Young, and G. S. Frankela, “Aluminum alloy corrosion inhibition by vanadates”, Journal of Electrochemical Society, 153 12 (2006) B533-B541
96. A. N. Salak, J. Tedim, A. I. Kuznetsova, M. L. Zheludkevich and M. G.S. Ferreira, “Anion exchange in Zn–Al layered double hydroxides: In situ X-ray diffraction study”, Chemical Physics Letters 495 (2010) 73–76
97. G. Contini, A. Ciccioli, C. Cozza, M. Barbaro and A.M. Marabini, “Infrared study of 2-mercaptobenzothiazole and two of its derivatives adsorbed on PbS”, International Journal of Mineral Processing 51 (1997) 283-291
98. M. Del Arco, E. Cebadera, S. Gutiérrez, C. Martín, M.J. Montero, V. Rives, J. Rocha and M.A. Sevilla, “Mg,Al Layered Double Hydroxides with Intercalated Indomethacin: Synthesis, Characterization, and Pharmacological Study”, Journal of pharmaceutical sciences 93 (2004) 1649-1658
99. F. Prinetto, G. Ghiotti, P. Gra and D. Tichit, “Synthesis and characterization of sol-gel Mg/Al and Ni/Al layered double hydroxides and comparison with co-precipitated samples”, Microporous and Mesoporous Materials 39 (2000) 229-247
100. T. Qi, Y. Zhang, X.Zhang, P.Yuan,and H. He, “Synthesis and Characterization of Layered Double Hydroxides with a High Aspect Ratio”, Journal of Solid State Chemistry 179 (2006) 708-715
101. L. Lv, “Defluoridation of drinking water by calcined MgAl-CO_3 layered double hydroxides”, Desalination 208 (2007) 125–133
102. M. Reis, F. Tronto and J. Valim, “Effects of pH, temperature, and ionic strength on adsorption of sodium dodecylbenzenesulfonate into Mg–Al–CO_3 layered double hydroxides”, Journal of Physics and Chemistry of Solids 65 (2004) 487–492

103. H.- S. Kim, T. Kimura, T. Kudo, I. Homma and Y. Amazaki, “Synthesis and Conducting Properties of Hydroxylcontaining LDH for Alkaline Membrane”, The Electrochemical Society 215th ECS Meeting abstract 316

104. C. Li, L. Wang, D. G. Evans and X. Duan, “Thermal Evolution and Luminescence Properties of Zn-Al-Layered Double Hydroxides Containing Europium(III) Complexes of Ethylenediaminetetraacetate and Nitrilotriacetate”,Industrial and Engineering Chemistry Research. 48 (2009) 2162–2171

105. C. O. Oriakhi, I. V. Farr and M. M. Lerner, “Thermal characterization of poly(styrene sulfonate)/layered double hydroxide nanocomposites”, Clays and Clay Minerals 45 2 (1997) 194-202

106. T. Kuehn and H. Poellmann, “Synthesis and characterization of Zn-Al layered double hydroxides intercalated with 1- to 19-carbon carboxylic acid anions”; Clays and Clay Minerals 58 5 (2010) 596–605

107. Z. P. Xu and H. C. Zeng, “Abrupt structural transformation in hydrotalcite-like compounds $Mg_{1-x}Al_x(OH)_2(NO_3)x \cdot nH_2O$ as a continuous function of nitrate anions”, Journal of Physical Chemistry B 105 (2001) 1743–1749

108. I. Crespo, C. Barriga, M. A. Ulibarri, G. González-Bandera, P. Malet and V. Rives, “An X-ray Diffraction and Absorption Study of the Phases Formed upon Calcination of Zn-Al-Fe Hydrotalcites”, Chemistry of Materials 13 (2001) 1518-1527

109. A. Ennadi, A. Legrouri, A. De Roy and J. P. Besse, “X-Ray Diffraction Pattern Simulation for Thermally Treated [Zn-Al-Cl] Layered Double Hydroxide”, Journal of Solid State Chemistry 152 (2000) 568-572